

# BARC

## NEWSLETTER

### IN THIS ISSUE

- Engineering Abiotic Stress Tolerance in Transgenic Banana Plants by Overexpressing Effector/ Transcription Factor Genes
- Development of Thermal Neutron Detector based on Lithium TetraBorate (LTB) Single Crystal
- Installation and commissioning of an Automatic Solar Radiation Monitoring System (ASRMS)
- New Hot Cell Facility for Post Irradiation Examination
- Microbial Bioremediation of Uranium- An Overview



*Celebrating the spirit of Diamond Jubilee Year*

Department of Atomic Energy Tableau in the 66<sup>th</sup> Republic Day Parade 2015 at Rajpath, New Delhi



### *Atoms in the Service of the Nation*

Celebrating its diamond jubilee year, the Department of Atomic Energy (DAE) portrays in its tableau, its expertise in harnessing the tremendous potential of the atom for the benefit of the society. The tableau is led by a white dove atop an atomic orbital symbolizing the conviction of the nation in spreading the message 'Atoms for Peace'. It also pays homage to the visionary Dr. Homi Jehangir Bhabha, founding father of the Indian Nuclear Programme. The trailer portion of the tableau is conceptually divided into three parts depicting peace, progress and prosperity, vis-a-vis the service deliverables of the Department. The first part symbolizes progress in the field of medical technology depicting the indigenously developed 'Bhabhatron' machine, used in radiotherapy and delivering affordable health care. The colourful flora, following it, showcases prosperity in food and agriculture through mutation breeding technology to provide disease-resistant and high yielding seeds and food irradiation techniques that increase the shelf life of the produce. Lastly, standing tall, the indigenous Nuclear Reactor highlights the advantage of nuclear energy to provide an unlimited supply of clean and green energy for the sustained progress of the nation.

***Department of Atomic Energy***

## CONTENTS

|  |    |
|--|----|
| <b>Editorial Note</b>  | ii |
| <b>Brief Communications</b>  |    |
| • Thiourea Application Boosts Crop Productivity and helps in Understanding of Redox Regulatory Mechanism in Plants<br><i>Bio-Science Group</i>   | 1  |
| • <sup>177</sup> Lu-DOTA-TATE, a Radiotherapeutic Agent for Treatment of Neuroendocrine Cancers<br><i>Radiochemistry &amp; Isotope Group</i>   | 3  |
| <b>Research Articles</b>   |    |
| • Engineering Abiotic Stress Tolerance in Transgenic Banana plants by Overexpressing Effector/Transcription Factor Genes<br>U.K.S. Shekhawat and T.R. Ganapathi<br><i>Nuclear Agriculture and Biotechnology Division</i>                         | 5  |
| • Development of Thermal Neutron Detector based on Lithium Tetraborate (LTB) Single Crystal<br>G.D. Patra, A.K. Singh, B. Tiwari, S.G. Singh, D.G. Desai, M. Tyagi, S. Sen, S.C. Gadkari and S.K. Gupta<br><i>Technical Physics Division</i>     | 9  |
| <b>Technology Development Articles</b>   |    |
| • Installation and Commissioning of an Automatic Solar Radiation Monitoring System (ASRMS)<br>Ananta Joshi and R.J. Patel<br><i>Refuelling Technology Division</i>   | 14 |
| • New Hot Cell Facility for Post Irradiation Examination<br>Anil Bhandekar, K.M. Pandit, M.P. Dhotre, P. Nagaraju, B.N. Rath, Prerna Mishra, Sunil Kumar, J.S. Dubey, G.K. Mallik and J.L. Singh<br><i>Post Irradiation Examination Division</i> | 19 |
| <b>Feature Articles</b>  |    |
| • Microbial Bioremediation of Uranium- An Overview<br>Celin Acharya<br><i>Molecular Biology Division</i>   | 27 |
| • Meteorological Analysis of Very Severe Cyclonic Storm Hudhud in and around BARC Visakhapatnam in October 2014<br>A. Vinod Kumar, R. Jana, N. S. Krishna and T. Sambamurty<br><i>Radiation Safety Systems Division</i>                          | 31 |
| <b>News &amp; Events</b>   |    |
| • Third National Symposium on Advances in Control and Instrumentation (SACI- 2014): a Report   | 36 |
| • 29 <sup>th</sup> Training Course on "Basic Radiological Safety and Regulatory Measures for Nuclear Facilities": a Report   | 37 |
| • National Safety Day Celebration at BARC  | 38 |
| <b>BARC Scientists Honoured</b>  | 39 |

## Editorial Committee

### Chairman

Dr. S.M. Sharma,  
Associate Director, Physics Group

### Co-Chairman

Dr. G.K. Dey,  
Associate Director, Materials Group

### Editor

Dr. G. Ravi Kumar  
Head, SIRD

### Associate Editors for this issue

Dr. S.K. Sandur, RB&HSD  
Dr. K.G. Bhushan, TPD

### Members

Dr. G. Rami Reddy, RSD  
Dr. A.K. Tyagi, Chemistry Divn.  
Dr. S.M. Yusuf, SSPD  
Dr. S. Kannan, FCD  
Dr. C.P. Kaushik, WMD  
Dr. S. Mukhopadhyay, Seismology Divn.  
Dr. A.K. Bhattacharjee, RCnD  
Dr. B.K. Sapra, RP&AD  
Dr. J.B. Singh, MMD  
Dr. K.G. Bhushan, TPD  
Dr. S. Mukhopadhyay, ChED  
Dr. S.K. Sandur, RB&HSD  
Dr. Smt. S.C. Deokattey, SIRD

## From the Editor's Desk

Welcome to the second issue of the BARC Newsletter for 2015. Five articles and two Brief Communications have been featured in this issue.

One of the communications highlights a radiotherapeutic agent developed in BARC for the treatment of neuroendocrine cancers, which has benefited more than one thousand patients so far. One of the articles projects Ag doped Lithium tetraborate crystals as an alternative to the  $^3\text{He}$  based neutron detectors.

Reliable performance of nuclear fuels and critical core components is essential for efficient life management of nuclear facilities. A new hot cell was commissioned and activated recently in BARC for post irradiation examination of nuclear fuels and structural components. The salient features of this facility have been detailed in one of the technology development articles.



Dr. G. Ravi Kumar

On behalf of the Editorial Committee

## Thiourea Application Boosts Crop Productivity and helps in Understanding of Redox Regulatory Mechanism in Plants

Bio-Science Group

In the face of challenges of food security and climate change, sustainable agriculture has emerged as key principle to nurture healthy ecosystems and support good management of land, water and natural resources. Under a collaborative program with Rajasthan Agriculture University (Bikaner, India), we have developed the application of thiourea as an easy and cost-effective technology for boosting crop productivity under farmer's field conditions. Thiourea is an organo-sulfur compound with formula  $SC(NH_2)_2$ . It is structurally similar to urea except that oxygen atom is replaced by a sulfur atom. Thiourea applicability has also been demonstrated for increasing grain filling under drought and

arsenic stress conditions in Indian mustard and rice, respectively (Fig. 1). At physiological level, this is associated with enhanced metabolite translocation from source (leaves) to sink (pods) (Srivastava et al., 2008) and co-ordinated regulation of plant's source-to-sink relationship (Pandey et al., 2013).

Apart from applied perspective, ROS scavenging action of thiourea is also utilized for understanding the significance of redox regulatory mechanisms associated with different abiotic stresses in plants. In our laboratory, we have developed the application of thiourea a tool to pinpoint the genes, miRNAs and other physiological and biochemical mechanisms which are directly regulated through cellular redox status. This is preferred over widely used redox probe GSH, as being a non-physiological thiol, gene expression changes associated with thiourea are more closely associated with redox state. Using thiourea as a tool, we have successfully identified the redox associated candidate genes associated with calcium and ABA signaling (Srivastava et al., 2010a) and plant-water homeostasis (Srivastava et al., 2010b) in mustard. We have also extended our study to identify redox regulatory mechanisms associated with arsenic stress tolerance and accumulation in rice (Srivastava et al., 2014).

Our future research is to utilize thiourea based research to advance our understanding of plant stress tolerance mechanisms and to provide effective, sustainable solutions to avoid crop losses under changing climatic conditions and enhance productivity.

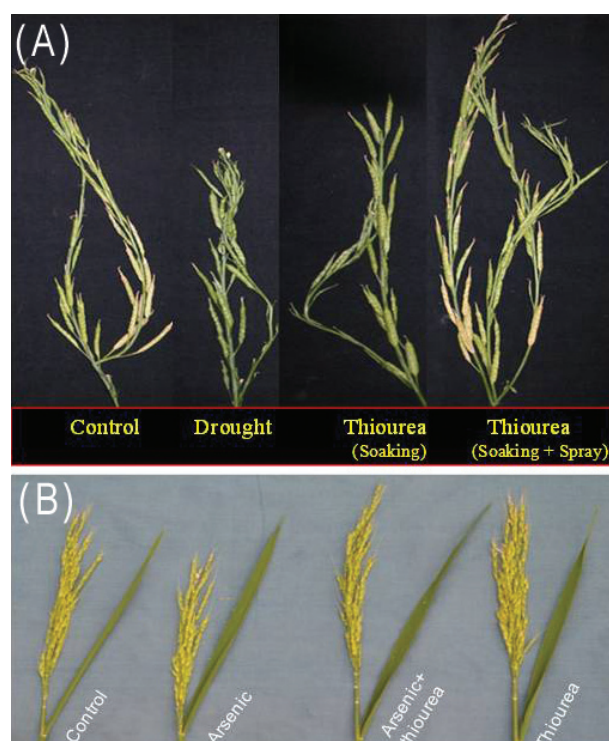


Fig. 1: Impact of thiourea application on agriculture. Thiourea application improves the performance of mustard and rice under drought (A) and arsenic (B) stress conditions

**References:**

1. Srivastava AK, Nathawat NS, Ramaswamy NK, Sahu MP, Singh G, Nair JS, Radha Krishna P, D'Souza SF (2008) Evidence for the thiol induced enhanced in situ translocation of <sup>14</sup>C-Sucrose from source to sink in Brassica juncea. *Environmental and Experimental Botany* 64, 250–255.
2. Pandey M, Srivastava AK, D'Souza SF and Suprasanna P (2013) Thiourea, a ROS scavenger, regulates source-to-sink relationship for enhanced crop yield and oil content in Brassica juncea (L.). *PloS One* 8(9): e73921.
3. Srivastava AK, Ramaswamy NK, Suprasanna P and D'Souza SF (2010a) Genome-wide analysis of thiourea modulated salinity-stress responsive transcripts in seeds of Brassica juncea L: Identification of signaling and effector components of stress tolerance. *Annals Of Botany* 106, 663-674.
4. Srivastava AK, Suprasanna P, Srivastava S, D'Souza SF (2010b) Thiourea mediated regulation in the expression profile of aquaporins and its impact on water homeostasis under salinity stress in Brassica juncea roots. *Plant Science* 178, 517-522.
5. Srivastava AK, Srivastava S, Mishra S, Suprasanna P, D'Souza SF (2014) Identification of redox-regulated components of arsenate (AsV) tolerance through thiourea supplementation in rice. *Metallomics* 6, 1718-1730.

## <sup>177</sup>Lu-Dota-Tate, a Radiotherapeutic Agent for Treatment of Neuroendocrine Cancers

### Radiochemistry & Isotope Group

Peptide Receptor Radionuclide Therapy (PRRT) employing radiolabeled somatostatin analog peptides, particularly <sup>177</sup>Lu-DOTA-TATE (<sup>177</sup>Lu-labeled DOTA coupled Tyr3-Octreotate Figure-1), is now an established therapeutic modality for the treatment of patients suffering from a wide variety of inoperable neuroendocrine cancers over-expressing somatostatin receptors. In the last decade, PRRT has gained momentum and at present is being routinely used as a therapeutic regimen in a limited number of countries. India, with a large population, has a significant number of patients who require PRRT

and this need to be provided at a reasonable cost due to the limited affordability of a large mass of population. The challenge associated with PRRT using <sup>177</sup>Lu-DOTA-TATE lies in its preparation with adequately high specific activity so that the required dose could be administered to the cancerous lesions without saturating the limited number of receptors available on the target. Since the radiopharmaceutical is prepared at the hospital radiopharmacy, just prior to administration in patients, the available specific activity of <sup>177</sup>Lu at the time of preparation should be considered for formulation of the agent with

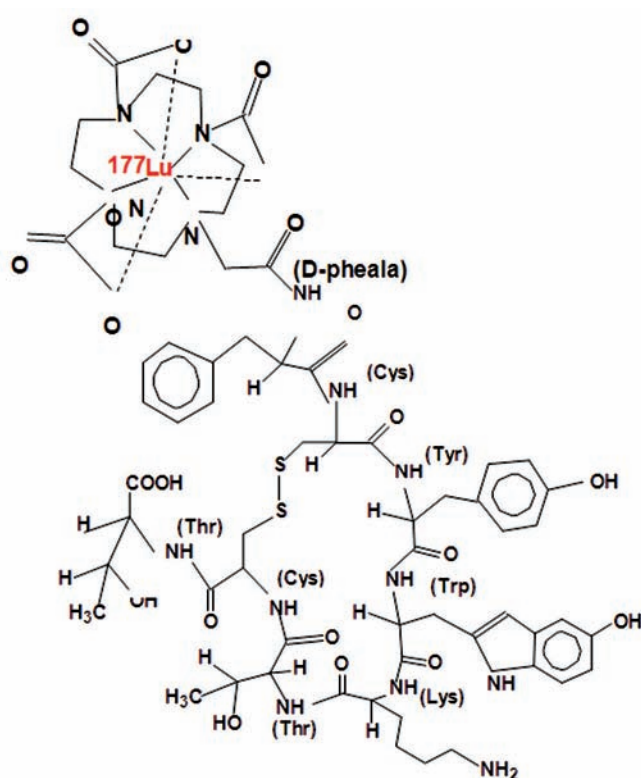


Fig. 1: Structure of <sup>177</sup>Lu-DOTA-TATE



Fig. 2: Whole-body scintigraphic image of a neuroendocrine cancer patient treated with 7.4 GBq of <sup>177</sup>Lu-DOTA-TATE

highest specific activity and thus ensuring maximum therapeutic efficacy. Accordingly, a suitable method for the 'in-situ' preparation of patient dose of  $^{177}\text{Lu}$ -DOTA-TATE was developed in 2007 in our laboratory using the  $^{177}\text{Lu}$  produced in BARC. This therapeutic modality was introduced for the first time in India in 2008 for the treatment of cancer patients in collaboration with Department of Nuclear Medicine, All India Institute of Medical Sciences (AIIMS), New Delhi. Subsequently, to cater to the need of increasing number of cancer patients, PRRT has been started in nine other nuclear medicine centres across our country and more than 1000 patients (on an average 3-4 doses per patient) have benefitted from this therapeutic modality till date. To simplify the

protocol for preparation of this radiopharmaceutical at the user end, we have developed a freeze-dried kit of DOTA-TATE in 2012, for the preparation of up to 7.4 GBq patient dose of  $^{177}\text{Lu}$ -DOTA-TATE. This single-vial kit, which enables a convenient and single-step preparation of the agent using  $^{177}\text{Lu}$  having specific activity  $\geq 740 \text{ MBq}/\mu\text{g}$ , has been successfully used for the treatment of patients in a couple of nuclear medicine centres in India. Further clinical evaluation of the freeze-dried DOTA-TATE kit is presently being pursued in collaboration with our clinical partners. Awareness of the effectiveness of PRRT and consequently the interest for use of  $^{177}\text{Lu}$ -DOTA-TATE is increasing in India.

# Engineering Abiotic Stress Tolerance in Transgenic Banana plants by overexpressing Effector/ Transcription Factor Genes

**U.K.S. Shekhawat and T.R. Ganapathi**  
Plant Cell Culture Technology Section,  
Nuclear Agriculture and Biotechnology Division

## Abstract

Banana (*Musa spp.*) is the most important fruit worldwide. Among the factors which are responsible for lower productivity in banana plantations, abiotic stress factors like water limitation, soil salinity and temperature extremes are the most significant. We have attempted to use transgenic approach for development of abiotic stress tolerant banana plants. In this pursuit, we have overexpressed multiple abiotic stress related native gene sequences in transgenic banana and characterized the responses of the resulting transgenic plants in response to application of simulated abiotic stress conditions. Physiological and biochemical assays performed on these transgenic plants have proved the efficacy of using this approach to develop abiotic stress tolerant banana plants.

## Introduction

Modern-day plants have evolved over hundred of years from simple organisms in response to continuous abiotic and biotic environmental alterations. Among the abiotic cues that have affected plant evolution, water availability, soil salt content and incidence of extreme temperatures are the most important. In order to survive these challenges to their survival, plants have developed the capacity to react to these external signals by using specialized physiological and biochemical strategies. Upon stress perception, plants activate a cascade of cellular events involving several signal transduction pathways that lead to modification levels of specific transcription factors resulting in the up- or down-regulation of specific genes responsible for synthesis of effector proteins and/ or metabolites which contribute to stress tolerance.

Banana is the most important fruit crop in the world. It also fulfills a huge food security role for millions of people mainly in the African continent. India is the largest producer of banana in the world with a production of 28.45 million tonnes from an area of

0.796 million hectares with a productivity of 35.7 MT/ha. Bananas are especially susceptible towards any sort of water scarcity and in fact they rarely attain their full genetic yield potential due to limitations imposed by water availability. A shallow root system together with a permanently green canopy comprising of large leaves and numerous stomata translates into enormous water requirements for the banana plant. Additionally, bananas are also sensitive to soil salinity and low temperatures.

We have been studying multiple banana abiotic stress related transcription factors as well as effector genes in order to engineer abiotic stress tolerance in transgenic banana plants. Some of the genes characterized are briefly described in the following sections.

### Banana Dehydrin (*MusaDHN-1*)

Dehydrins are highly hydrophilic proteins which are known to be involved in playing adaptive roles in abiotic stress conditions which have dehydration as a common component. We identified a novel banana SK3-type dehydrin, *MusaDHN-1* from

banana EST database maintained at NCBI and later characterized this dehydrin by overexpressing it in transgenic banana plants (Shekhawat et al. 2011). In native untransformed banana plants MusaDHN-1 was found to be induced in leaves and roots by drought, salinity, cold, oxidative and heavy metal stress and by treatment with abscisic acid, ethylene and methyl jasmonate. This inducible expression in abiotic stress conditions indicated its involvement in stress tolerance in banana plants. MusaDHN-1 promoter was isolated from banana genomic DNA by employing TAIL-PCR technique. Promoter analysis performed by constructing a MusaDHN-1 promoter:  $\beta$ -glucuronidase fusion construct and its transformation in tobacco leaf discs confirmed the abiotic stress inducibility of MusaDHN-1. Transgenic banana plants which were conformed to overexpress MusaDHN-1 constitutively were found to be phenotypically normal in their growth and development. When these plants were subjected to drought and salt-stress treatments in in vitro and ex vitro assays, they performed better than the equivalent controls. Biochemical analysis of these transgenic plants showed enhanced accumulation of proline and reduced malondialdehyde levels in stress conditions.

#### **Banana Stress Associated Protein (*MusaSAP1*)**

A20/AN1 zinc finger domain containing Stress Associated Proteins (SAP) are known to be involved in different stress response pathways in higher plants. We have identified a novel banana SAP gene, MusaSAP1, in banana EST database and this gene was subsequently characterized by carrying out its overexpression in transgenic banana plants (Sreedharan et al. 2012). Expression profiling of MusaSAP1 performed in native untransformed plants indicated that it was up-regulated by drought, salt, cold, heat and oxidative stress and by treatment with abscisic acid. To confirm the cellular localization of this protein a Musa-SAP1::GFP fusion protein was designed and transformed into onion peel cells using

*Agrobacterium* mediated genetic transformation. The fluorescence analysis indicated that MusaSAP1 is incompletely translocated to nucleus. Gene copy number analysis of MusaSAP1 performed by real time PCR and Southern blotting showed that MusaSAP1 gene occurs as a single copy per 11 chromosome set in banana nucleus. Transgenic banana plants which constitutively overexpressed MusaSAP1 were phenotypically indistinguishable from the untransformed controls and also displayed better stress tolerance features as compared to equivalent controls in both in vitro and ex vivo assays. Further, strong up-regulation of a polyphenol oxidase (PPO) coding transcript seen in MusaSAP1 overexpressing plants along with induction of MusaSAP1 by wounding and methyl jasmonate treatment pointed towards probable involvement of MusaSAP1 in banana biotic stress responses where PPOs are expected to perform major functions in multiple defense pathways.

#### **Banana bZIP transcription factor (*MusabZIP53*)**

bZIP transcription factors have been shown to be involved in diverse cellular processes in plants. We identified a bZIP gene, MusabZIP53, from banana EST database and later characterized it by overexpressing in transgenic banana plants of cultivar Rasthali (Shekhawat et al. 2014). This gene was found to be upregulated in native untransformed banana plants in response to cold and drought stress and also by ABA treatment in both leaf and root tissues. Transgenic banana plants which constitutively overexpressed MusabZIP53 showed prominent growth retardation from very early stages of banana transformation/regeneration procedure and later the mature greenhouse hardened transgenic plants were found to display a distinct dwarf phenotype. These transgenic plants showed differential regulation of genes belonging to several families known to be involved in abiotic stress perception and mitigation. These included genes responsible for dehydration response element binding proteins, late embryogenesis abundant proteins, anti-oxidant

enzymes, aquaporins, polyphenol oxidases, Aux/ IAA proteins and some of the proteins involved in amino acid metabolism. We detected a strong up-regulation of four polyphenol oxidase coding genes in MusabZIP53 overexpressing plants together with high induction of these transcripts in native banana leaves by cold stress and ABA treatments which pointed towards potential involvement of MusabZIP53 in the master control of polyphenol oxidase activity in banana plants.

**Banana Plasma Membrane Intrinsic Protein (*MusaPIP2;6*)**

High soil salinity is considered to be a major abiotic stress for plants and it is an important limiting factor in nurturing of crop plants worldwide. We identified an aquaporin gene, *MusaPIP2;6* and characterized it by overexpressing in transgenic banana plants (Sreedharan et al. 2015). *MusaPIP2;6* was initially identified using a comparative study of stressed and

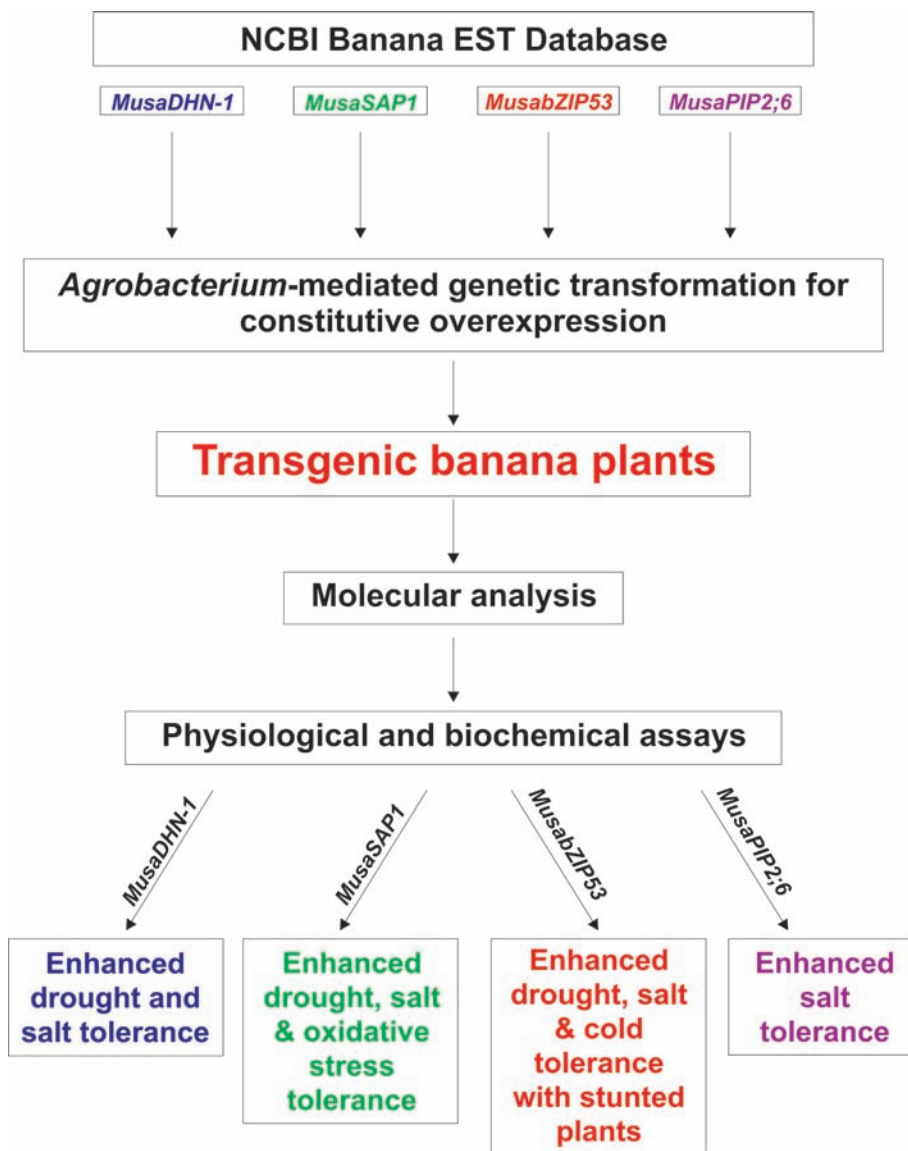


Fig. 1: Schematic representation of development of abiotic stress tolerant transgenic banana plants using four native banana genes.

non-stressed banana tissues derived EST databases. Its overexpression in transgenic banana plants was undertaken to study its probable functions in banana. It was found that overexpression of MusaPIP2;6 in transgenic banana plants by employing a constitutive or an inducible promoter (pMusaDHN-1) lead to higher salt tolerance in comparison with equivalent untransformed control plants. To confirm the exact cellular localization of MusaPIP2;6 protein we used transiently transformed onion peel cells and found that MusaPIP2;6 protein tagged with GFP was translocated to the cellular plasma membrane. MusaPIP2;6-overexpressing transgenic banana plants displayed comparatively better photosynthetic efficiency (Fv/Fm ratios) and lower membrane damage (MDA equivalents) under salt stressed conditions.

### Conclusion

The characterization studies performed on four genes in our laboratory over the last couple of years prove the efficacy of using native genes for development of abiotic stress tolerant transgenic banana plants (Figure 1). Apart from abiotic stress tolerance banana plants, we have also developed disease resistance establishing the versatility of our approach. We plan to demonstrate the efficacy of transgenic banana

lines developed in our laboratory through limited field trials in near future.

### References

1. Shekhawat UKS, Ganapathi TR, Srinivas L (2011) MusaDHN-1, a novel multiple stress-inducible SK3-type dehydrin gene, contributes affirmatively to drought- and salt-stress tolerance in banana. *Planta* 234:915–932.
2. Sreedharan S, Shekhawat UKS, Ganapathi TR (2012) MusaSAP1, a A20/AN1 zinc finger gene from banana functions as a positive regulator in different stress responses. *Plant Mol Biol* 80:503–517.
3. Shekhawat UKS, Ganapathi TR (2014) Transgenic banana plants overexpressing MusabZIP53 display severe growth retardation with enhanced sucrose and polyphenol oxidase activity. *Plant Cell Tiss Org Cult* 116:387–402.
4. Sreedharan S, Shekhawat UKS, Ganapathi TR (2015) Constitutive and stress-inducible overexpression of a native aquaporin gene (MusaPIP2;6) in transgenic banana plants signals its pivotal role in salt tolerance. *Plant Mol Biol* (In press) DOI: 10.1007/s11103-015-0305-2.

# Development of Thermal Neutron Detector based on Lithium Tetraborate (LTB) Single Crystal

G.D. Patra, A.K. Singh, B. Tiwari, S.G. Singh, D.G. Desai, M. Tyagi, S. Sen,  
S.C. Gadkari and S.K. Gupta  
Technical Physics Division

## Abstract

High quality single crystals of Ag doped lithium tetraborate ( $\text{Li}_2\text{B}_4\text{O}_7:\text{Ag}$ ) have been grown using the Czochralski technique. The presence of naturally abundant  $^6\text{Li}$  and  $^{10}\text{B}$  in the crystal has been gainfully utilized to fabricate compact devices to measure thermal neutron fluxes from various sources. To achieve a high signal-to-noise ratio, a thermally stimulated luminescence (TSL) measurement set-up has been developed using a solar-blind PMT that has a matching response with the emission from  $\text{Ag}^+$  ions. The measurements were carried out ex-situ as well as in real-time.

## Introduction

Neutron detectors are essential tools used in various fields like nuclear power, nuclear medicine, particle physics, magnetism, etc. Currently, thermal neutron detection relies on gas-filled high pressure tube based detectors containing either Helium-3 ( $^3\text{He}$ ) or Boron Trifluoride ( $\text{BF}_3$ ) gases [1]. These gas-filled detectors require high bias voltages and use either toxic  $\text{BF}_3$  or rare  $^3\text{He}$  gases. Though  $^3\text{He}$  is ideal for high pressure gas-based neutron sensors owing to its high capture cross-section for thermal neutrons, yet this state-of-the-art detector is bulky and difficult to configure. Further,  $^3\text{He}$  isotope has extremely low natural abundance and mostly produced as a byproduct of nuclear device manufacturing. The production of nuclear weapons has been drastically reduced over the past few decades leading to a shortage in  $^3\text{He}$  supply [2]. Therefore the demand for alternate thermal neutron detectors is continuously increasing due to the above challenges.

In search for an alternative to the  $^3\text{He}$  gas-filled neutron detections, certain points need to be considered: a neutron is an electrically neutral particle that interacts only with a nucleus, so the material for its detection

must contain an element with a high neutron capture cross-section. In order to be detected, this interaction must produce charged particles. There are few isotopes that meet these criteria:  $^6\text{Li}$  ( $n,\alpha$ ) ( $\sigma = 938\text{b}$ ),  $^{10}\text{B}$  ( $n,\alpha$ ) ( $\sigma = 3845\text{b}$ ), and  $^{nat}\text{Gd}$  ( $n,\beta$ ) ( $\sigma = 49153\text{b}$ ).  $^{nat}\text{Cd}$  also has a high neutron capture cross-section (2520 b), but does not produce any charged particle, therefore is not useful for detector applications. Elements with lower atomic numbers are preferable in order to reduce gamma ray absorption. The solid state detectors are more advantageous due to their higher atomic density (compact size and much higher efficiency compared to gas-filled detectors) and stability for a prolonged useful life. An intensive search for a  $^3\text{He}$  gas-based neutron detector replacement yielded new technologies like organic liquid scintillators containing Li, B, or Gd, thin film neutron absorber coatings for semiconductor devices and for gas discharge counting tubes. Research on a few materials like  $^6\text{Li}$ -glass:Ce,  $^6\text{LiF}/\text{ZnS}:\text{Ag}$ ,  $\text{LiBaF}_3:\text{Ce},\text{K}$ ,  $\text{LiBaF}_3:\text{Ce},\text{Rb}$ ,  $^6\text{LiI}:\text{Eu}$ ,  $\text{Cs}^6\text{LiYCl}_6:\text{Ce}$ ,  $^6\text{Li}^{dep}\text{Gd}(\text{}^{11}\text{BO}_3)_3:\text{Ce}$ ,  $^6\text{Li}^{dep}\text{Gd}(\text{}^{11}\text{BO}_3)_3:\text{Ce}$ , etc. is currently at the fore front to develop alternative materials that could replace  $^3\text{He}$  gas-filled neutron [3,4].

Lithium tetraborate [ $\text{Li}_2\text{B}_4\text{O}_7$ (LTB)] is a promising material for the detection of thermal neutrons due to

the presence of  ${}^6\text{Li}$  and  ${}^{10}\text{B}$  (with a possibility to further improve the performance using enriched materials). In addition, the lower atomic number also imparts some gamma transparency to the material. LTB is a well known dosimetric material and a lot of literature is available for its TSL response to different doses of  $\gamma$  and  $\beta$  radiations [5]. For neutron detection, LTB in the form of single crystals has advantages compared to other forms as it has high density, broad transmission range, better mechanical hardness, better energy proportionality and higher resolution.  ${}^6\text{Li}$  and  ${}^{10}\text{B}$  in the LTB interact with neutrons to produce energetic charged particles. Subsequently these charged particles deposit their energies resulting in the generation of electron and holes that are trapped in trap centers present in the material. The absorbed dose information may be retrieved by heating the samples in a thermally stimulated luminescence (TSL) read out set-up. Thus, the neutron flux could be measured both in passive mode (neutron dosimetry [6],[7]) by ex-situ heating of the sample after the neutron exposure and in real-time by collecting the signal with a continuous heating of the sample during the neutron exposure.

In this article we describe the growth of LTB:Ag single crystals and development of a TSL set-up to measure thermal neutron flux ex-situ as well as in real-time.

### Single Crystal Growth

Single crystals of LTB:Ag were grown by the Czochralski method. An automatic diameter controlled crystal puller (Oxypuller, Cyberstar) was used for the growth of crystals [8]. Commercially available LTB polycrystalline powder material (99.998% pure, Aldrich make) was used as a starting charge. Activator Ag ions were mixed with the LTB starting charge in the form of high purity  $\text{Ag}_2\text{O}$ . To optimize the Ag concentration, LTB crystals with different amounts of  $\text{Ag}_2\text{O}$  in the range from 0.1 to 1.1 wt.% were grown. Li and B were taken in their natural abundance without further enrichment of  ${}^6\text{Li}$  and  ${}^{10}\text{B}$ . A platinum crucible

of 40 mm diameter was used for the growth. After several growth experiments, the growth parameters were optimized. The best crystals were grown at a pull rate of 0.2 mm/h and a rotation rate of 10 rpm with a high longitudinal thermal gradient of about 70-80°C/cm. This enabled the growth of clear, core-free, transparent crystals of 20-25 mm diameter and 20-30 mm length (as shown in Fig.1). The crystal ingot was cut into disks of different thickness and polished for various characterizations. A few samples of size 6 mm  $\times$  6 mm  $\times$  0.6 mm were cut from the polished crystal discs for neutron detection.

All the grown crystals showed good transmission of about 85% in the visible range indicating a good optical quality of the grown crystals. The X-ray powder diffraction (XRD) confirmed the phase purity of the grown crystals. Ag is incorporated as  $\text{Ag}^+$  ions in the LTB lattice as indicated by the presence of absorption band at  $\sim 205$  nm corresponding to the  $4d^{10} \rightarrow 4d^9 5s$  transition of  $\text{Ag}^+$  centers [8]. All Ag-doped LTB crystals showed strong emission band at about 270 nm on excitation at 205 nm. This emission is corresponding to the  $(4d^9 5s \rightarrow 4d^{10})$  transition of  $\text{Ag}^+$  ions. The optimum concentration of silver doping was found to be around 1.0 wt.% in the melt for the best TSL response [9].



Fig. 1: As-grown LTB:Ag crystal ingot.

### TSL Read Out Set-Up for Neutron Dosimetry

It is always desirable to get higher sensitivity for a dosimeter material. To accomplish this, the luminescence must be well matched with the spectral response of the photo-detector in a TSL readout system. We had earlier found that the emission band of LTB:Ag at 270 nm [9] does not match well with the spectral response of conventional photo-multiplier tubes (PMT). Therefore, an ET make 9422B solar blind PMT having a spectral response in the range from 110 to 360 nm was employed as the photo-detector in an in-house developed TSL detection set-up. This read-out set-up was used for recording the TSL glow curve of the LTB:Ag crystal samples exposed to various radiations like gamma-rays and neutrons. Recently, we have shown that this modified TSL readout set-up could measure a gamma dose as low as  $3 \mu\text{Gy}$  with a minimum detectable dose in the sub-micro Gy range [9]. Using this read out system we have recently found that LTB:Ag is a very promising dosimeter material for  $\gamma$  and  $\beta$  rays. The same set-up was used for thermal neutron detection.

### Neutron Dosimetry

For neutron dosimetry first LTB:Ag crystals were irradiated with thermal neutrons and the TSL glow curve of irradiated samples was recorded using the TSL set-up. For neutrons exposure, few samples of size  $6 \text{ mm} \times 6 \text{ mm} \times 0.6 \text{ mm}$  were irradiated with thermal neutrons ( $\lambda: 5\text{\AA}$ ) of about  $10^6 \text{ n/s/cm}^2$  flux through a 2 mm slit (neutron beamline at the Dhruva reactor, BARC). Exposure for different time periods was given to get different fluences. Thereafter, TSL glow curves were recorded at a constant heating rate of  $1^\circ\text{C/s}$ . The TSL curve for all the neutron irradiated samples showed a peak at about  $160^\circ\text{C}$ , similar to gamma irradiation [9,10]. Fig.2. shows the response of the material from a very low fluence to high fluence ( $1.0 \times 10^6 \text{ n/cm}^2$ ). The TSL response of the material is found to be linear in this fluence range. To predict the low fluence detection limit,

the data range has been extrapolated. The extrapolated curve shows that a fluence of less than  $100 \text{ n/cm}^2$  can be easily detected with the present set-up.

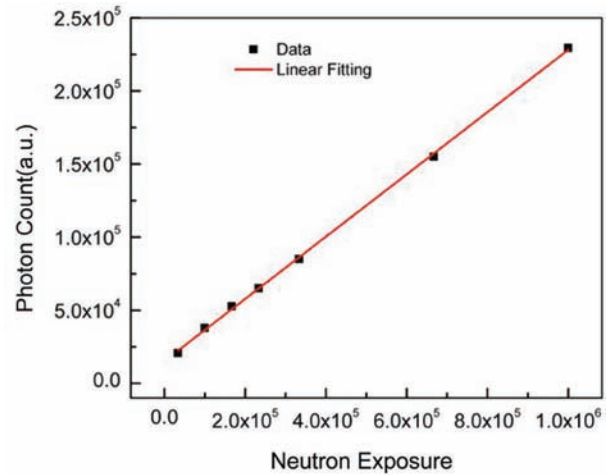


Fig. 2: Response of LTB:Ag crystal to different neutron exposures.

To demonstrate the ability to distinguish different low neutron fluxes, the single crystal pieces were exposed for an hour to two different fluxes of 150 and  $250 \text{ n/s/cm}^2$  (at RPAD, BARC). During these experiments, contribution from gamma background has been taken into account. The gamma background was the same for both the neutron fluxes, as the source was the same. To remove the gamma contribution, a lead block of 50 mm thickness was used in front of the single crystal pieces for the both fluxes. The TSL glow curves for two different fluxes are shown in the Fig.3. The peak height for the two fluxes is

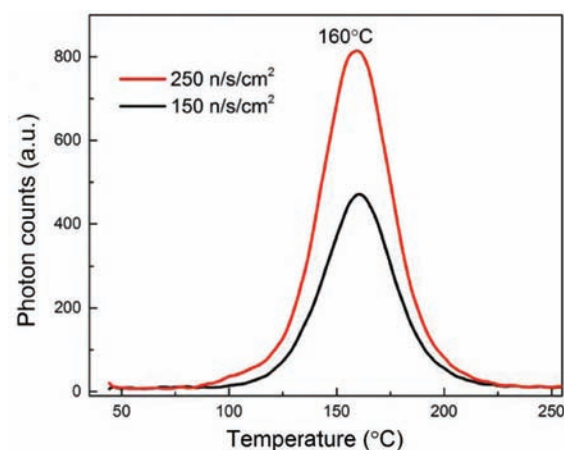
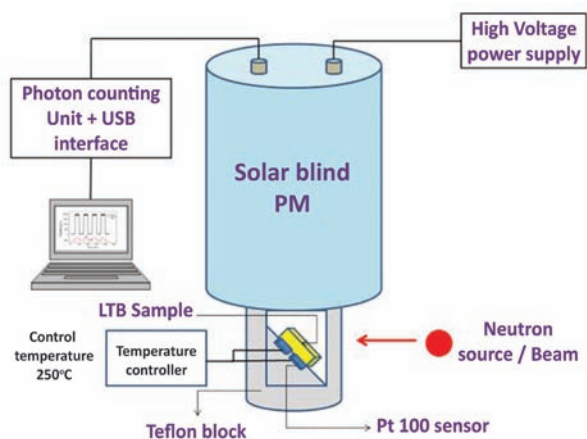


Fig. 3: TSL glow curve of LTB:Ag for two different neutron fluxes.

different and the ratio of the integrated area of the two peaks is measured as 1.6 which is very close to the calculated ratio of 1.67. Here the calculated ratio means the ratio of two different neutron fluxes of 250 and 150 n/s/cm<sup>2</sup> (i.e. 250/150=1.67). Thus the crystal can easily distinguish between two different low level neutron fluxes.

**In-Situ Real Time Thermal Neutron Detection**

For real-time monitoring of neutrons, a detector system has been developed by fixing two Pt-100 thermal sensors (working both as heater and temperature sensor) on a small LTB:Ag (6x6x0.6 mm<sup>3</sup>) plate. To protect the PMT from direct exposure to the neutron beam, the LTB plate was placed in a 45° reflecting geometry, as shown in Fig.4.



**Fig. 4: Schematic diagram of the set-up to detect thermal neutrons in real-time.**

This set-up was tested on a thermal neutron beamline at the Dhruva reactor, BARC. A flux of about 10<sup>6</sup> n/s/cm<sup>2</sup> was incident through a 2.0 mm slit on the LTB:Ag crystal. To reduce gamma background, a 50 mm thick lead shield was used in front of the detector. Temperature of the LTB:Ag plate was kept constant at about 250°C by adjusting the current passing through Pt-100 as the TSL glow-peak for LTB:Ag is in the 150-200°C range. This heating ensured the detrapping of electrons from the Ag<sup>+</sup> trap centers immediately after being populated by charge carriers.

These charge carriers are produced by alpha/charged-particles generated due to (n,α) reactions at <sup>6</sup>Li and <sup>10</sup>B nuclei in LTB crystals. During the experiment, a borated rubber sheet was used as a shutter to fully stop the thermal neutron beam. The current from the PMT was recorded in DC mode as a function of time. Fig.5 shows the response of the PMT when the LTB:Ag crystal is exposed to thermal neutrons. The use of borated rubber sheet in front of the set-up blocked the thermal neutrons allowing the measurement of gamma contribution from the Pb(n,γ) reaction. But in this condition no count in the detector set-up was observed i.e. the gamma contribution was submerged within the noise of the system. The signal (counts) comes down to near zero instantaneously after the neutron beam was stopped and again comes back to the original value when the shutter is removed. Using this set-up, a neutron flux of less than 1000 n/s/cm<sup>2</sup> can be measured in real-time.

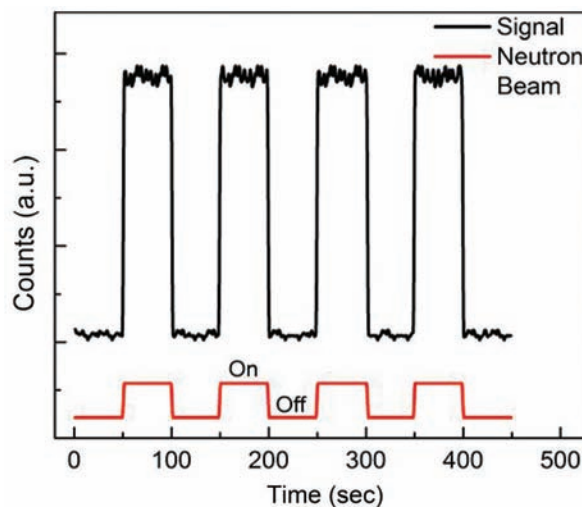


**Fig. 5: Real-time detection of thermal neutrons using an LTB:Ag crystal mounted on Pt-100 heaters. The PMT current is plotted as a function of time as the thermal neutron beam was switched ON/OFF using a borated rubber shutter.**

**CONCLUSIONS**

High optical quality single crystals of LTB with silver as an activator were grown. This material was used as a neutron sensing material using an in-house made TSL read-out system with a solar blind PMT as a photo

detector. The samples were tested with sources of neutrons and small variation in the neutron flux was easily measured using the TSL glow curve. The detection of neutrons was also demonstrated in real-time using the LTB:Ag crystal heated at about 250°C. The sensitivity of this material can be further enhanced by using LTB material enriched in  $^6\text{Li}$  and  $^{10}\text{B}$ .

### Acknowledgement

Authors are grateful to Head, RPAD and Head, SSPD for allowing to conduct experiments using various neutron sources.

### References

1. R. T. Kouzes, J. R. Ely, A. T. Linteur, and D. L. Stephens, PNNL-18903, " PNNL Report, 2009.
2. R.T Kouzes, Report PNNL-18388, Dept. of Energy (2009)
3. C.W.E. van Eijk, *Nucl. Instr. and Meth. A* 460 (2001) 1.
4. C.W.E. van Eijk, A. Bessiere, P. Dorenbos *Nucl. Instr. and Meth. A* 529 (2004) 260.
5. Babita Tiwari, N. S. Rawat, D. G. Desai, S. G. Singh, M. Tyagi, P. Ratna, S. C. Gadkari, and M. S. Kulkarni, *J. Lumin.* 130 (2010) 2076.
6. H Ing, *Radiation Measurements.* 33 (2001) 275.
7. Francesco D'Errico, Ravinder Nath, Giovanni Silvano, Luigi Tana, *International Journal of Radiation Oncology\*Biology\*Physics* 41, (1998) 1185.
8. G.D. Patra, Mohit Tyagi, D.G. Desai, Babita Tiwari, Shashwati Sen, S.C. Gadkari. *J. Lumin.* 132 (2012) 1101.
9. G.D. Patra, S.G. Singh, A.K. Singh, M. Tyagi, D.G. Desai, B. Tiwari, S. Sen, S.C. Gadkari, *J. Lumin.* 157 (2015) 333.
10. A. T. Brant, B. E. Kananan, M. K. Murari, J. W. McClory, J. C. Petrosky, V. T. Adamiv, Ya. V. Burak, P. A. Dowben, and L. E. Halliburton, *J. Appl. Phys.* 110 (2011) 093719.

## Installation and Commissioning of an Automatic Solar Radiation Monitoring System (ASRMS)

**Ananta Joshi and R.J. Patel**  
Refuelling Technology Division

Good quality, reliable solar radiation data is extremely important for all research activities in solar energy applications. Photovoltaic (PV) and Concentrating Solar Power (CSP) systems need accurate solar radiation information for the performance evaluation both in short term and long term. In different solar technology research, improvements in the performance of technologies (e.g. PV/CSP) are often small and incremental, but the total and cumulative gain can be large. Different technological solutions may show different efficiencies under ideal laboratory simulation. However, this needs to be verified in real time under varying weather and sky conditions compared to 'reference' quality solar radiation measurements.

Hence, for any solar technology development or product quality control, it is extremely important to measure the solar radiation accurately. In order to maximise operating efficiency of a plant or system, solar radiation monitoring instruments at the plant provide the irradiance data to assess the efficiency of the energy generation chain. Using high quality solar radiation measurements at the plant, a database of performance can be built up, allowing more accurate forecasting of the future energy yield.

The Ministry of New and Renewable Energy (MNRE) has undertaken the programme of implementing the objectives of the Jawaharlal Nehru National Solar Mission launched by the Govt. of India. It is observed that in the last two decades, there has been significant reduction in solar Direct Normal Irradiance (DNI) in most of the regions in India as per the research work published by scientists [1, 2, and 3]. This phenomenon is termed as Solar Dimming. It was suggested that any informed decision on Solar

thermal or Concentrated Photovoltaic technologies cannot be taken without inputs on future DNI at sight with a good degree of confidence.

The task of exploring this issue further was taken up by the Refueling Technology Division (RTD) of BARC. Subsequently, a detailed survey was carried out in this regard. The above mentioned research findings were traced to the papers published in the year 2009-10 in the *Journal of Geophysics*, wherein, scientists had published the analysis and results of their research work from the data collected from the Indian Meteorology Department (IMD) stations on the Solar Dimming phenomenon [1, 3]. However, due to lack of enough solar irradiance data in all parts of India, all the regions could not be covered for the analysis.

The Ministry of New and Renewable Energy (MNRE), Government of India has launched a nation-wide network of Solar Radiation Resource Assessment (SRRRA) stations in phases. This project is being implemented by the National Institute of Wind Energy (NIWE), Chennai, an autonomous R & D institution under the Ministry, because of its rich experience in Wind Resource Assessment and development of Wind Atlas for the nation. Under this project, over 100 SRRRA stations have been commissioned during 2012-13 and these are uniformly located to cover the entire country for proper assessment of solar resources.

An Automatic Solar Radiation Monitoring System (ASRMS), manufactured by GEONICA, Spain, was integrated and installed by RTD at Engineering Hall-7 roof top, BARC, for XII plan project on "Technology development for solar tower power plant". The purpose of this system is to continuously

monitor, collect and communicate the solar radiation parameters to a Central Receiving Station (CRS) located at control room of Hall-7, BARC for solar radiation resource assessment. The measured radiation data in real time will be utilized to evaluate the efficiency of prototype solar test facility installed at Hall-7 roof top. This system will also be used for evaluation of efficiency of other test facilities planned to be installed at Gamma Garden, BARC. For present application, this system has a Field Station at the roof top with full communication and data receiving, archiving and analysis facility at a Receiving Station at Hall-7 control room.

The field station will continuously measure Global Horizontal Irradiance (GHI), Diffuse Horizontal Irradiance (DHI) and Direct Normal Irradiance (DNI). Referring to the Fig. 1, DNI is the solar irradiance that passes through directly to the earth's surface falling on a surface normal to the sun beam, DHI is the solar irradiance that is scattered out of the direct sun beam and falling on a horizontal surface and GHI is the Direct and the Diffuse component of sunlight falling together on a horizontal surface. The measurement of DNI is important for evaluation of Concentrating Solar Power (CSP) and Concentrating Photovoltaic (CPV) systems whereas GHI/DHI measurements help evaluate PV systems. Following Fig. 1 describes these terms pictorially.

This system has the following Instruments;

- a) Pyranometer for GHI measurement
- b) Shaded Pyranometer for DHI measurement
- c) Pyrheliometer for DNI measurement.

All the three instruments are calibrated with the instruments traceable to World Radiometric Reference (WRR) of World Radiation Center (WRC), Davos of WMO.

The system has a two-axis chronological Sun Tracker with its control system mounted with Pyranometers, shading disc and Pyrheliometer. The sun tracker continuously tracks the sun guided by an algorithm that calculates the sun's position, based on geographical location and the date and time and aligns itself with the sun for these measurements. The sun tracker control system along with its data acquisition system uses the values of Longitude, Latitude, Altitude and Solar time to calculate the position of sun for activating tracker motors for alignment with the sun in real time. Global Positioning System (GPS) Receiver is installed with this system to acquire the values of Longitude, Latitude, Altitude and Solar time of the location. The data logger in this system samples the data every second for all the

**Global Horizontal Irradiance (GHI) Diffuse Horizontal Irradiance (DHI)**

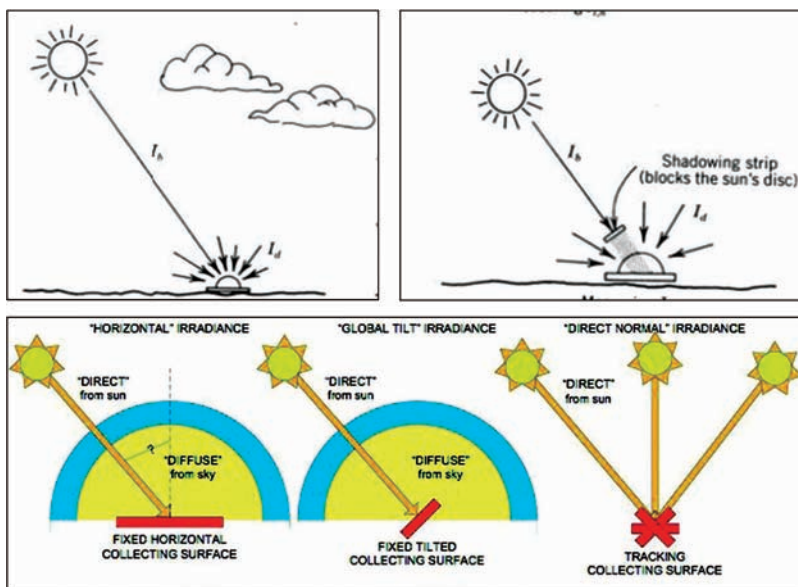


Fig. 1: GHI, DHI and DNI

parameters averaging every minute. It has a clock circuit that can be automatically synchronized by the GPS receiver, internally integrated with the unit's own electronic circuit and connected to an external antenna that receives time and position signals from a constellation of satellites (GLONASS and GPS). This time is used to calibrate the position of the Sun Tracker pointing arm vis-a-vis GPS solar timings. This permits clock precision of the order of nanoseconds, which is required for precisely synchronizing the pace of the clock. The Data logger

collects the data from the Instruments at the roof top and transfers to Receiving Station at Hall-7 control room. PV panels are used for power supply.

Pictures of the installed system (Figs. 2 and 3) and sample data (Figs. 4a thru 4d) of Solar irradiance measured hourly on specific days is shown.

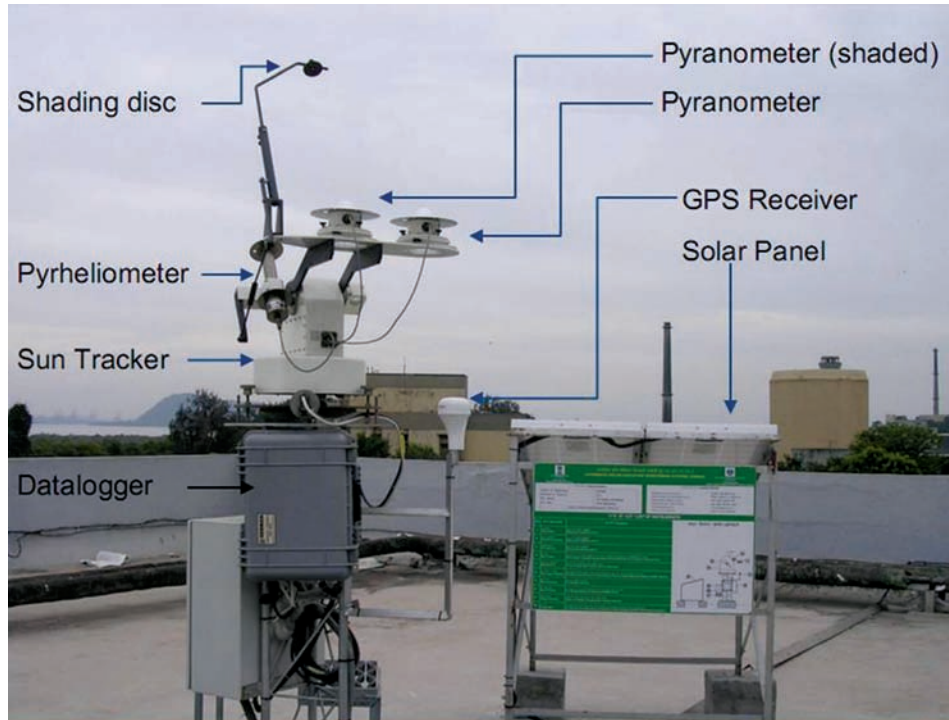


Fig. 2: Automatic Solar Radiation Monitoring System (ASRMS)

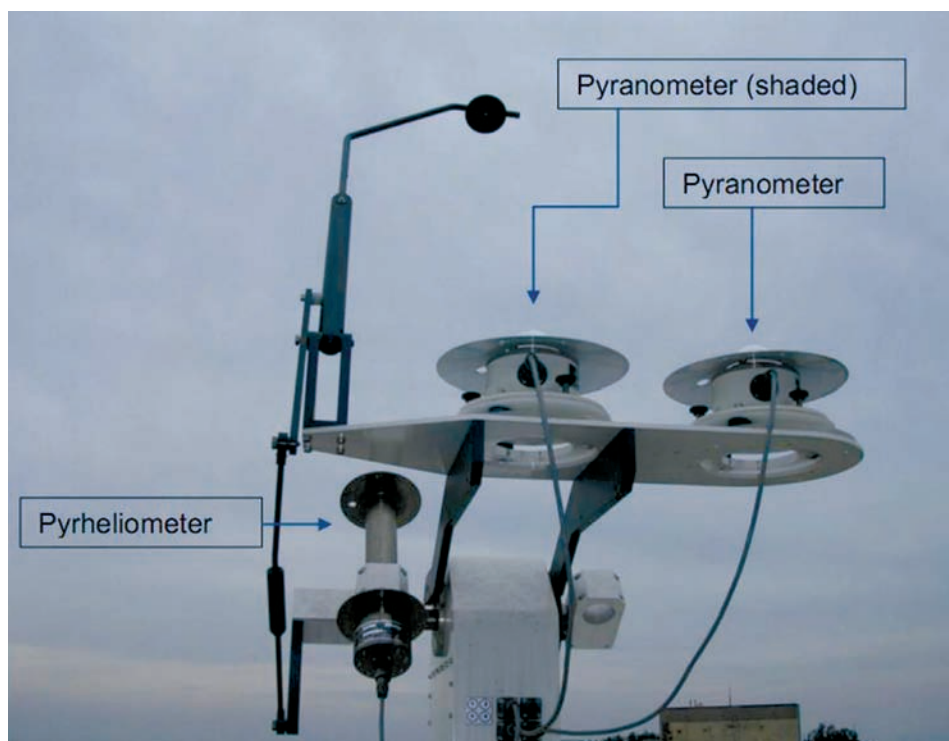


Fig. 2: Sensors for measuring GHI, DHI and DNI

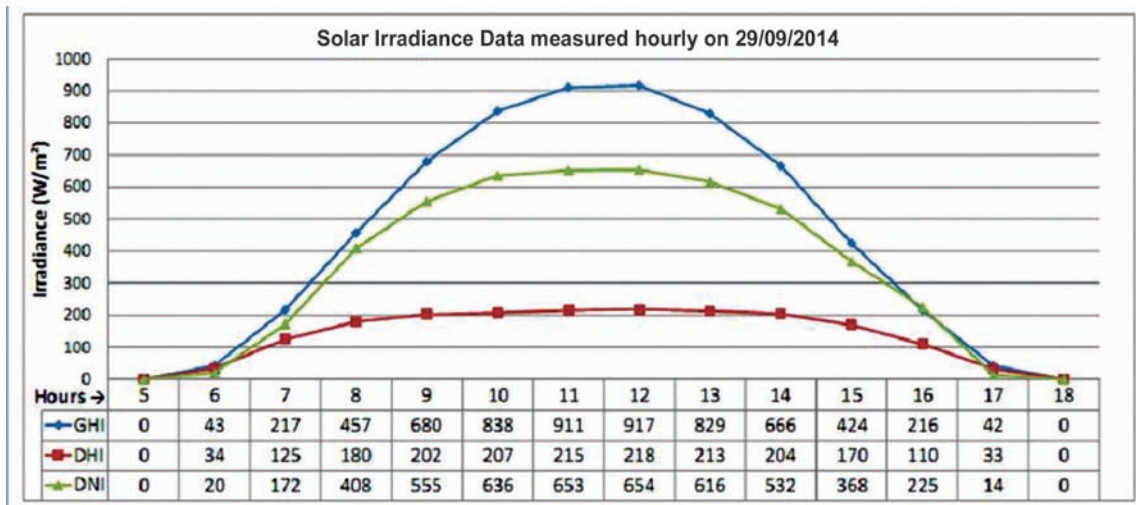


Fig. 4a: Sample data of Solar irradiance measured on specific day

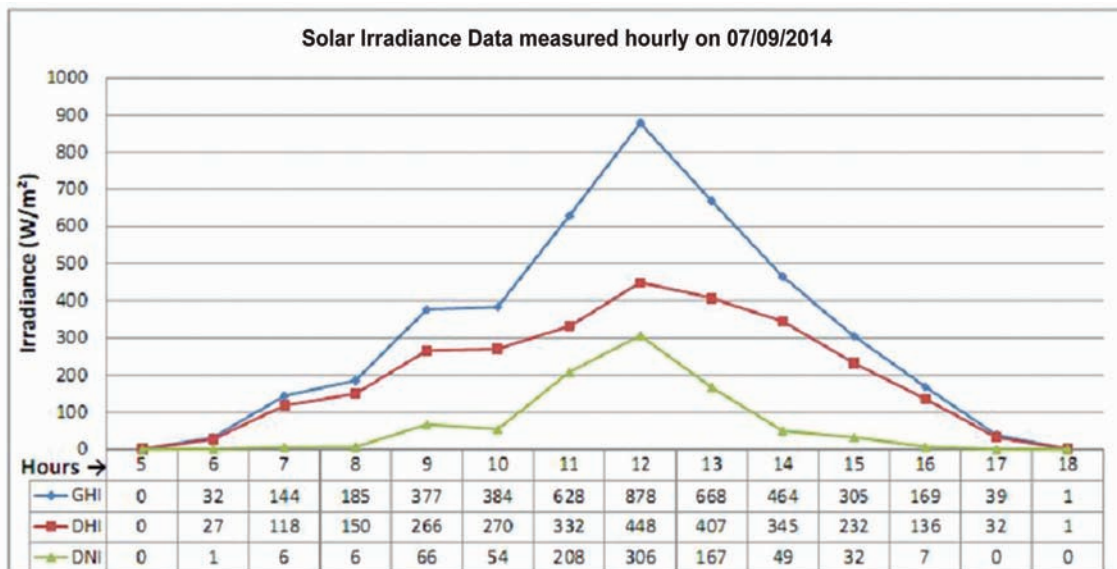


Fig. 4b: Sample data of Solar irradiance measured on specific day

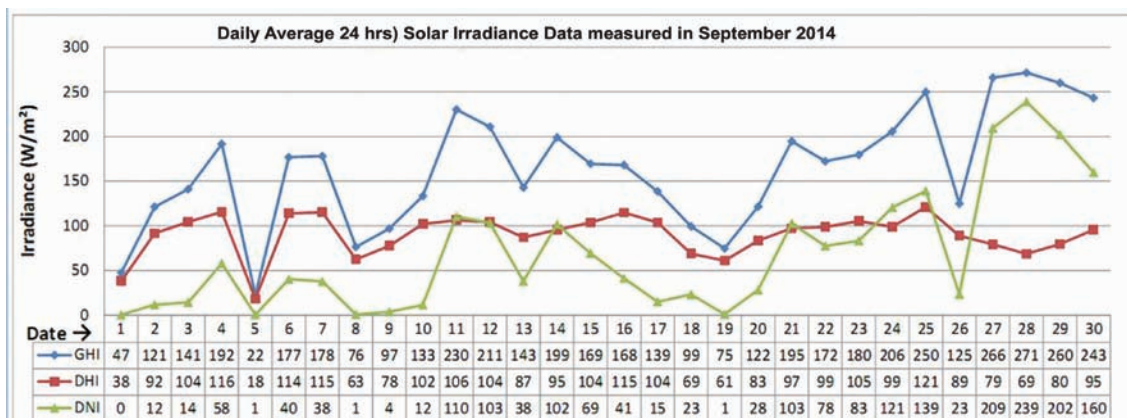


Fig. 4c: Sample data of Solar irradiance measured on specific month

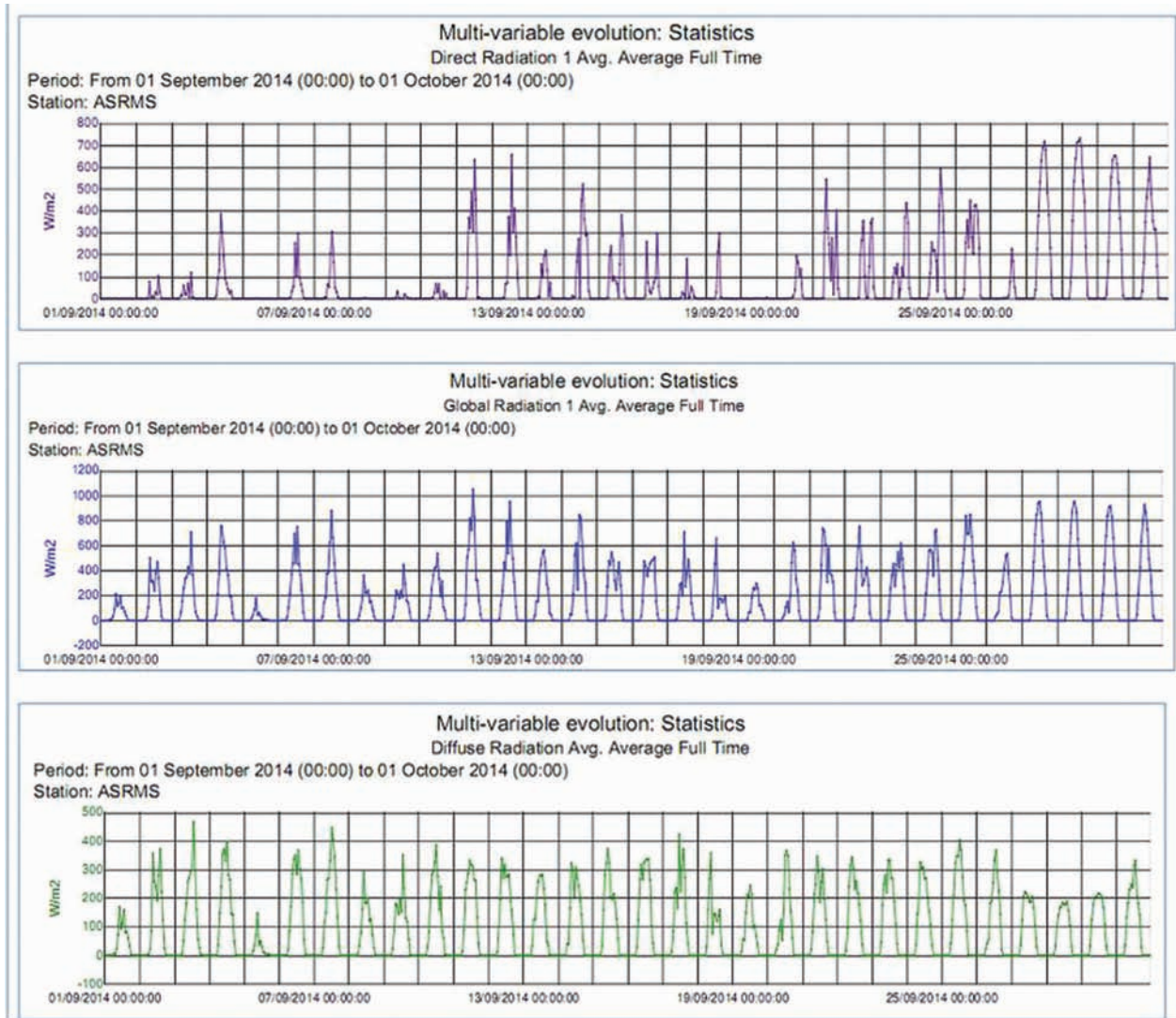


Fig. 4d: Sample data of Solar irradiance measured on specific month

The measurement of solar irradiance data by ASRMS in real time will help in performance evaluation of different solar technologies being developed in BARC and also in long term data acquisition for studies on effect of Solar Dimming.

#### References

1. Seminal role of clouds on solar dimming over the Indian monsoon region B. Padma Kumari and B.N. Goswami, *Geophysics Research Letter*, 37, L06703, 2010.
2. Solar dimming over the tropical urban region of Hyderabad, India: Effect of increased cloudiness and increased anthropogenic aerosols K.V.S. Badarinath, A.R. Sharma, D.G. Kaskaoutis, S.K. Kharol, and H.D. Kambezidis *J. Geophysics. Res.*, 115, D21208, 2010.
3. Observational evidence of solar dimming: Offsetting surface warming over India B. Padma Kumari, A.L. Londhe, S. Daniel, and D.B. Jadhav, *Geophysics. Research Letter*, 34, L21810, 2007.

## New Hot Cell Facility for Post Irradiation Examination

Anil Bhandekar, K.M. Pandit, M.P. Dhotre, P. Nagaraju\*, B.N. Rath, Prerna Mishra,  
Sunil Kumar, J.S. Dubey, G.K. Mallik, J.L. Singh  
Post Irradiation Examination Division  
\*Hot Lab Utilities & Engineering Services Section

### Abstract

The New Hot-Cells Facility (NHF) of Post Irradiation Examination Division (PIED) at RLG, BARC is designed for the Post Irradiation Examination (PIE) of irradiated nuclear fuels and structural components from research and power reactors. The NHF consists of two hot cells made of heavy density concrete and a number of lead cells. The hot cells are designed to handle  $\beta$ - $\gamma$  radioactivity. The lead cells in the facility are equipped with testing machines for evaluation of mechanical properties of irradiated materials. In addition, the facility will be also used for failure analysis of nuclear reactor components. This article describes the salient features of the hot cells and the PIE capabilities of the NHF.

### Introduction

Reliable performance of nuclear fuels and critical core components have a large bearing on the economics of nuclear power and radiation safety of the plant operating personnel. In view of this, PIE is periodically carried out on fuels and components to generate feedback information which is used by the designers, fabricators and the reactor operators to bring about suitable changes for improved performance of the fuel and components. Examination of the fuel bundles has to be carried out inside hot cells due to the high radioactivity associated with them. In the last four decades, post irradiation examination of different types of experimental as well as power reactor fuels and structural components used in the core of the reactor has been carried out in the old hot cells facility of the Post Irradiation Examination Division of BARC. The new

hot cell facility (NHF) has been designed, built and commissioned with additional features and capabilities, as an add-on facility to the old hot cells. A view of the operating area of the NHF is shown in Fig. 1. The hot cells at the NHF will cater to the PIE of a variety of irradiated fuels, core components and materials as given in Table 1. The facility will also be used for failure analysis of reactor components. An overview of the salient features and capabilities of the new hot cell facility at PIED is given in this article.



**Fig. 1: Operating area of the hot cells in the NHF showing the viewing windows and master slave manipulators**

**Table 1: List of fuels and components which can be examined in NHF**

|    |   |
|----|---|
| a. | NU fuel bundles and MOX fuel bundles from the PHWRs                   |
| b. | MOX fuel bundles and LEU bundles from the BWRs                        |
| c. | Experimental MOX fuels irradiated in research reactors                |
| d. | MOX/LEU fuel bundles from future PWRs                                 |
| e. | Fuels of research reactors & future reactors such as AHWR, CHTR, etc. |
| f. | Pressure tubes, Calandria tubes and End fittings of the PHWRs         |
| g. | Control blades of BWRs and Control elements of the PHWRs              |
| h. | Shut off rods of the PHWRs  |
| i. | Other core internals which are to be assessed                         |
| j. | Surveillance specimens from BWRs                                      |
| k. | Material irradiated for materials development programme               |

**New Hot Cell Facility (NHF)**

The new hot cell facility has two areas for handling radioactive materials. They are:

- Hot cells for handling highly radioactive irradiated fuels and structural materials

- Lead cells and low active laboratories for handling of specimens with a lower radiation field.

**Comparison of New and Old Hot Cells**

*Fuel transfer port size*

The old hot cells were designed for the PIE of fuel from CIRUS reactor. The cell has a 150 mm cylindrical port for introducing irradiated fuel/ structural component into the hot cell. This poses a limitation on the size of the fuel/component that can be introduced into the old hot cell. The new hot cells have a transfer port with the maximum opening of 500 mm x 500 mm section which will facilitate loading of larger components like LWR fuel assembly, control blade assembly, etc. into the cells for PIE. Fig. 2 shows the (a) cold side and (b) hot side of the fuel transfer port in the new hot cell.

*Cell dimensions*

The length of the hot cell in the NHF is 16.9 m as compared to 4.8 m in the old hot cell. This provides the advantage of examining longer components such as full length irradiated pressure tube, LWR fuel rods, etc. In the old hot cells, application of certain techniques such as seamless gamma scanning of long fuel elements like those of Dhruva was difficult.



**Fig. 2: (a) Cold side and (b) hot side of the transfer port in the new hot cell**

The NHF provides the facility of continuous scanning of longer fuel elements.

### **Shielding Capacity**

The shielding capacity of the old hot cells is up to  $10^5$  Ci of  $\text{Co}^{60}$ . The hot cells at the NHF are capable of handling higher activities up to  $2.5 \times 10^5$  Ci of  $\text{Co}^{60}$  or  $2.6 \times 10^6$  Ci of fission products.

### **Features of the New Hot Cells**

The NHF consists of two hot cells, namely Cell-1 & Cell-2 and is designed to handle  $\beta$ - $\gamma$  radiation. The front, rear and side walls of the cells are 1.5 m thick and are made of heavy density concrete (density=3.4 g/cc). The bigger cell (Cell-1) is 16.9 m long, 2.1 m wide and 4.7 m high and the smaller cell (Cell-2) is 5 m long, 2.1 m wide and 4.7 m high. All regions of Cell-1 and Cell-2 are provided with lead glass viewing windows, master slave manipulators (MSMs), ports for in-cell camera and service plugs, which are essential for carrying out PIE. Cell-1 is fitted with seven radiation shielding windows and seven pairs of rugged duty master slave manipulators. Cell-2 is fitted with two radiation shielding windows and two pairs of rugged duty master slave manipulators.

Cell-1 is provided with three personnel entry doors and Cell-2 with one personnel entry door. The roof of the hot cells is made of steel with rotating roof plug assemblies for introduction of heavy equipment and their removal. The rotating roof plug assemblies above the hot cells are shown in Fig. 3. The rotating roof plugs are eccentric to each other and have 250 mm diameter opening each, which can be positioned so as to gain access to any location within the cell. These openings can be used to deploy remotely operating tools to handle objects/equipments kept in the cells, which cannot otherwise be handled using MSMs.

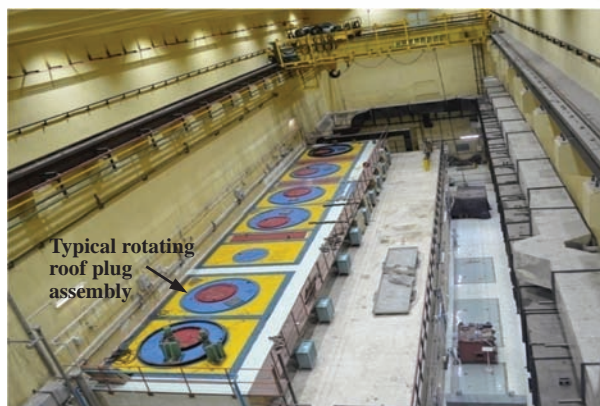


**Fig. 3: Hot cell roof with rotating roof plug assemblies**

Both cells have been provided with dedicated in-cell cranes of 2.0-ton capacity. The inter cell wall between Cell-1 and Cell-2 is provided with a shielded inter cell transfer drawer that can be used for transfer of material between the two cells. The rear walls of the cells are provided with external transfer drawers (ETDs) that can be used for transfer of material in and out of the hot cells. Both cells have a port on the sidewall in the warm work area to introduce irradiated materials into the cells. Tables of about 900 mm height are laid in the cells to provide the working surface. Various pipe lines are available within the cells. These lines can be used for providing services like compressed air, gas, vacuum etc. as per requirement. Three floor drains in Cell-1 and one in Cell-2 are provided to drain out the effluents to underground sump tanks located in the warm work area through a network of stainless steel pipe lines.

### **Ventilation in NHF**

The ventilation in the NHF is of once-through type and ensures dynamic confinement of radioactive particulates within the radioactive zones of the facility. The ventilation system is based on radioactive area zoning principles and satisfies the regulatory guidelines. The hot cells are provided with dedicated cell exhaust system for both Cell-1 and Cell-2; comprising of normal / standing blowers and High Efficiency Particulate Air (HEPA) filter banks. Radioactive

areas are also provided with separate lab exhaust and air supply system. Dust free cooled air is supplied in all radioactive area except hot cells. The hot cell is maintained at a negative pressure of 25 mm of water column (WC) with respect to operating area. There are 20 air changes per hour in the hot cells. The elaborate safety interlocks provided in the ventilation system ensure radiological safety of the plant personnel and public. Contaminated air passes through multiple HEPA filter banks before being released through the stack after monitoring, to ensure that the release of radioactivity in the environment is within the approved regulatory limits. The ventilation system is provided with data acquisition and monitoring system. Real time data of safety related parameters of ventilation such as negative pressure in hot cells, air changes per hour, pressure drop across HEPA filters etc. is monitored and logged in the central console located at operating area.

**Areas associated with the Hot Cells**

The facility is divided into four zones depending on the probability of radioactive contamination. The zones are coded white, green, amber and red,

with green having the lowest and the red having the highest probability of contamination. The white areas have a very remote chance of contamination by radioactivity. Fig. 4 gives the plan of the NHF showing the hot cells and associated areas.

The location of the operating area is shown in Fig. 4. Remote operations of equipment kept inside the hot cells are carried out from this area (see Fig. 1) using MSM and viewing windows. Control consoles of the in cell equipment and other measuring instruments are at kept in this area.

The isolation area is on the rear of the hot cells and acts as a buffer between the cells and the high bay surrounding the cells. The isolation area is provided with a 2T hand operated overhead travel underslung crane. The cell exhaust filters are located in nine separate pits below the isolation area floor.

The high bay surrounding the cells and isolation area on three sides is called the warm work area and houses a 40T/5T EOT crane. This area is used for receiving shielded casks containing radioactive materials. An airlock capable of accommodating a 30T trailer truck

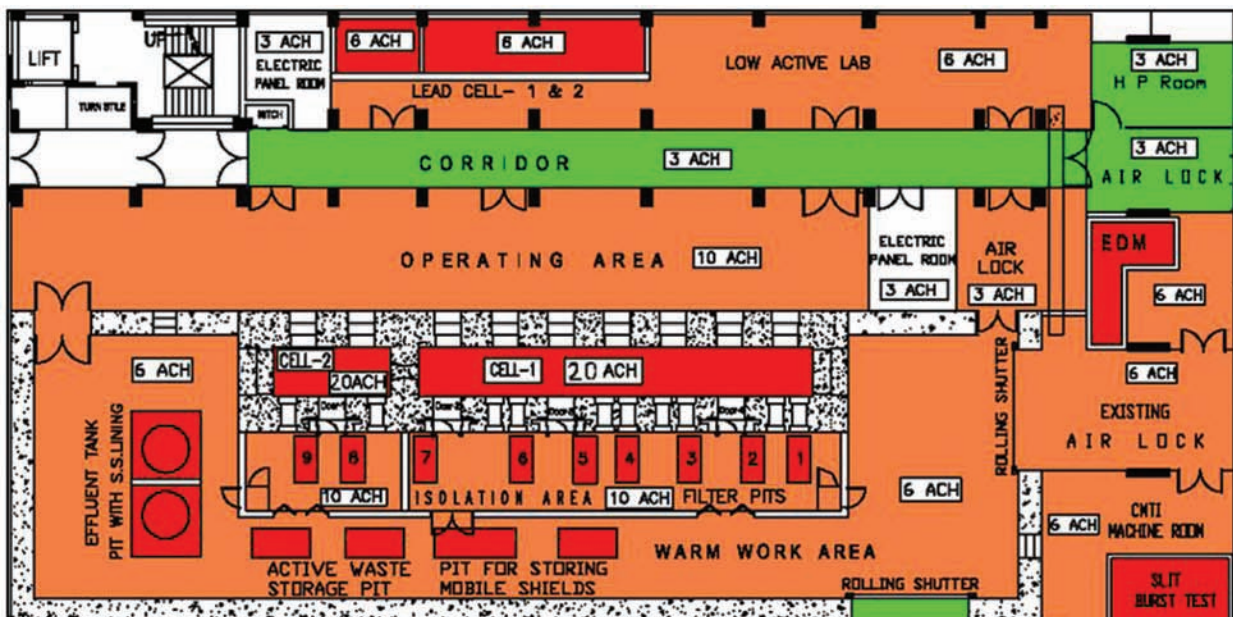


Fig. 4: Plan of the NHF showing the hot cells and the associated areas depicting appropriate health physics colour coding

is provided. Dollies running on rails are used to dock the cask to the transfer port of the hot cell (Fig. 5). Airlocks have also been provided for personnel entry into the warm work area.



**Fig. 5: Docking of the fuel transport cask with the fuel transfer port of the hot cell**

### **Lead Cells and Low Active Laboratories**

The low active laboratory is primarily used for carrying out mechanical tests on irradiated test specimens. Towards this an instrumented drop tower, servo hydraulic & screw driven universal testing machines, creep testing units and static load test setups have been installed in the low active laboratory. The front wall of the lead cells in this laboratory is made of 200 mm thick steel cased lead bricks and the rear walls are made of 100 mm thick lead bricks. The lead cells are fitted with articulated MSM, viewing windows, hatches/door for personnel entry, transfer ports and other handling facilities. The radioactivity of the test specimens will be limited to a few mCi of Co<sup>60</sup> equivalent.

### **PIE Capabilities**

The NHF has a comprehensive PIE facility in terms of material characterization and analytical capabilities required for PIE studies on nuclear fuels and materials. Various non destructive and destructive techniques are employed inside the hot cells for carrying out post irradiation examination on irradiated fuels. The PIE of irradiated PHWR fuel bundle is described in the following system to highlight the unit steps and capabilities of the hot cells.

### **Dismantling of the Fuel Bundle**

After preliminary survey of the fuel bundle for its overall integrity, the fuel bundle is dismantled to separate the fuel pins of the bundle for PIE investigations. Mechanical cutting machine using saw blade is installed in the hot-cells. Fig. 6 shows the dismantling of a fuel bundle using the mechanical cutting machine inside the hot cell as seen through the cell window.

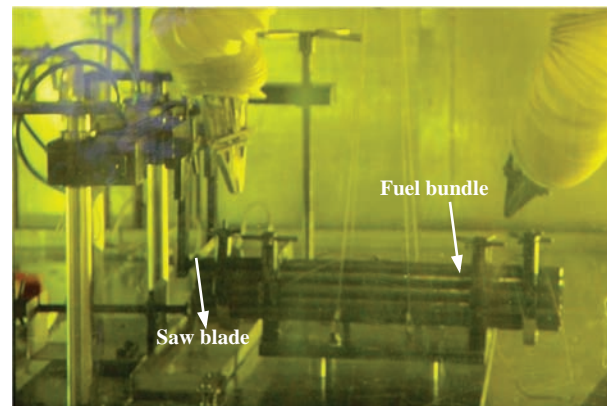


**Fig. 6: Saw blade based mechanical bundle dismantling machine installed inside the hot cells**

### **Visual examination**

Detailed visual examination of the fuel bundle and the pins is carried out inside the hot cells using a radiation resistant camera with pan tilt zoom (PTZ) facility. Surface conditions, such as abnormal distortion or deformation defects, damage on the fuel pin can be examined on the visual display placed in the operating area. Condition of the bearing pads and other welded appendages of the pins can also be examined.

### **Leak testing**

Leak testing of individual fuel pins is carried out using liquid nitrogen- alcohol leak test method. Fuel pin is first dipped inside a bath containing liquid nitrogen for a few minutes and then transferred to a bath containing alcohol, which is shown in Fig. 7 (a). In case of a fuel pin with a leak, the trapped liquid

nitrogen will bubble out, indicating the location of leak. Fig. 7 (b) shows bubbles emanating from a leak in one of the fuel pins.

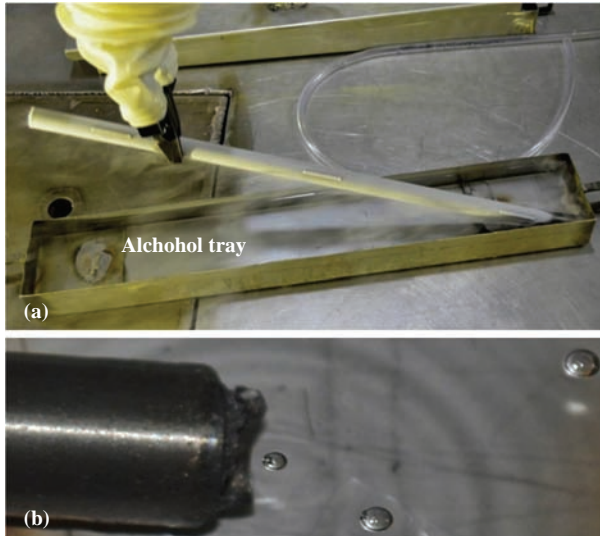


**Fig. 7: (a) Liquid nitrogen- alcohol leak testing set-up inside the hot cell and (b) Bubbles emanating from the failure location in the fuel pin**

**Profilometry**

A laser micrometer and a LVDT transducer based profilometer are used to determine the variation of the fuel pin diameter along its axis. Fig. 8 shows diametral profile measurement of a fuel pin using laser profilometer. The scanning stage used for movement of the fuel pin during LVDT transducer based profilometry is shown in Fig. 10.

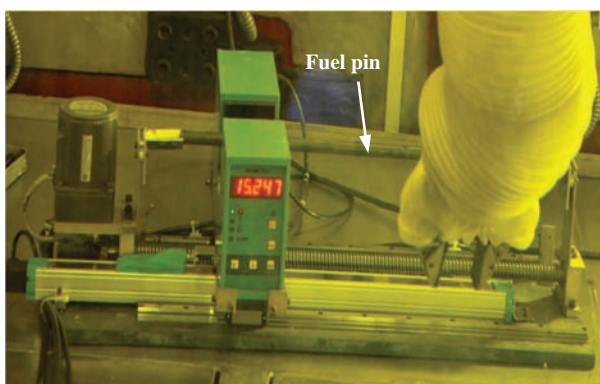


**Fig. 8: Laser profilometer inside the hot cell**

**Ultrasonic Testing**

Ultrasonic testing of fuel pins immersed in water in horizontal tank is carried out to detect the presence of incipient flaws in its cladding. The end plug welds are also inspected to detect deterioration of the weld and the heat affected zone. Fig. 9 shows the ultrasonic scanner fitted with probes for detection of axial and circumferential defects in the cladding.

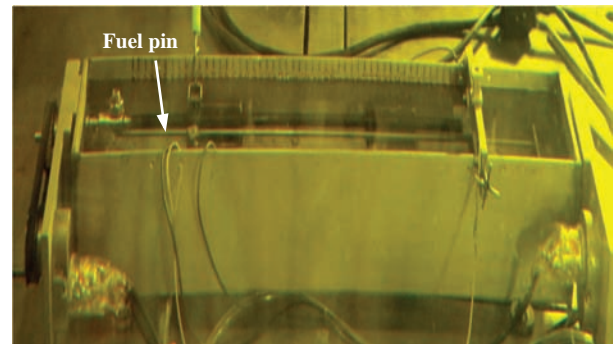


**Fig. 9: Ultrasonic testing set up installed in the hot cells**

**Gamma Spectroscopy and Scanning**

Gamma spectroscopy and gamma scanning using high resolution HPGe detector and multi channel analyser (MCA) are carried out on the irradiated fuel pins inside the hot cell. Co<sup>60</sup> and Cs<sup>137</sup> sources are used for energy calibration. The fuel pin is fixed on the scanning stage and gamma counting at various axial locations is carried out, with the detector placed in front of the collimator in the operating area. Relative burnup distribution in the fuel pin is measured by



**Fig. 10: Scanning stage for profilometry and gamma scanning inside the hot cells**

gamma scanning which uses  $Cs^{137}$  as the monitoring isotope for gamma counting. Fig. 10 shows the fuel pin loaded on the scanning stage inside the hot cells for gamma scanning.

### **Fission Gas Release measurement**

The released fission gas analysis set up is used for estimation of the quantity and composition of released fission gases inside the fuel pins. The setup essentially consists of a puncture chamber fixed inside the hot cell (Fig. 11), which is connected to the gas collection and measuring part located in the operating area, by means of stainless steel tubes. The estimation of parameters such as void volume of the fuel pin and the pressure and volume of the released gases is carried out by connecting calibration flasks to the system and by applying standard gas laws.

Chemical composition of the released gases is determined using a dual column gas chromatograph, with argon as the carrier gas. Thermal conductivity detector is used for the detection of the individual gases. A quadrupole mass spectrometer is used for measuring the isotopic ratios of Xe and Kr isotopes.

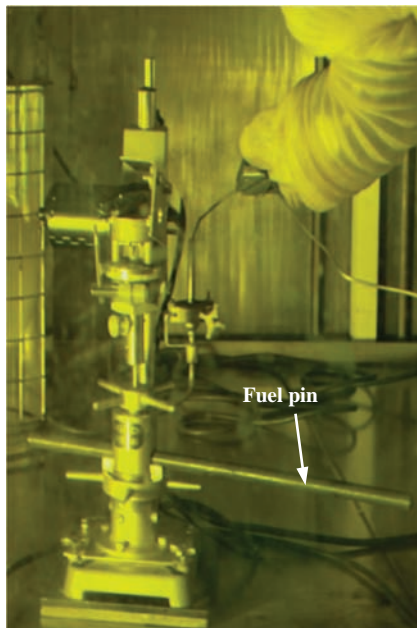


**Fig. 11: Puncturing set up in the hot cell for measurement of the fission gas release**

### **Preparation of Samples for Microstructural studies**

The changes in fuel microstructure during irradiation are studied by performing ceramography of the fuel sections. Cutting of fuel pins to get samples for metallography/ceramography may lead to falling off of fuel pieces due to the cracks developed during irradiation. Hence, the cut lengths of the fuel pins are impregnated with liquid Araldite using vacuum impregnation technique to keep the further fuel sections intact. Fig. 12 (a) shows the slow speed cut off machine placed inside the hot cell used for sectioning of the impregnated fuel pin. The slices cut from the impregnated piece of the fuel pin are mounted in SS rings. The mounted samples are then sequentially ground and polished on a grinder-polisher placed inside the hot cell, as shown in Fig. 12 (b).

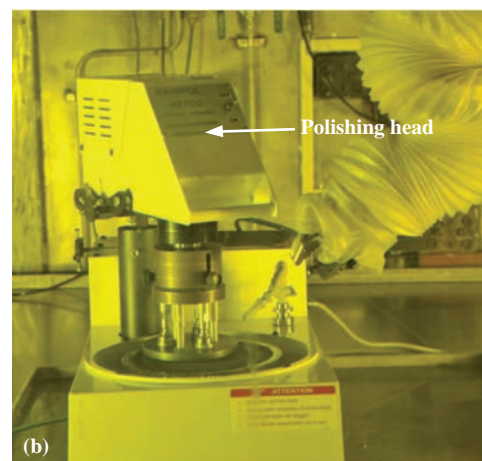
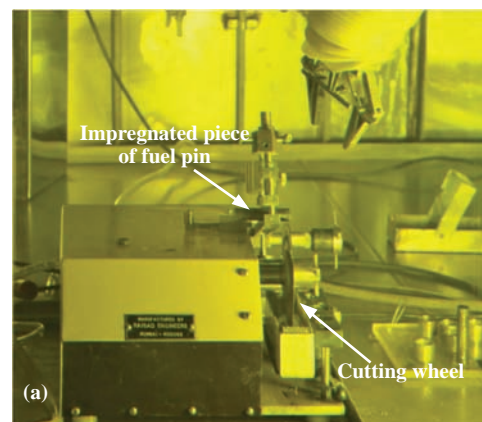


**Fig. 12: (a) Slow speed cut off machine for cutting of metallographic samples (b) Grinder polisher inside the hot cell**

### **Waste Management in NHF**

The solid and liquid radioactive wastes generated from the PIE activities in the facility are collected and sent to the Waste Management Division for necessary treatment and disposal. The gaseous waste is discharged after two stages of filtration to the atmosphere through the 75m high stack of Radiological Laboratories (RLG). The irradiated fuels and cut portions of fuel after completion of PIE will be packed in cans and sent for reprocessing.

### **Summary**

The new hot cell facility with the necessary equipments has been commissioned and activated for Post Irradiation Examination of irradiated nuclear fuels and structural components from research and power reactors. The results of PIE will provide valuable data

on fuel performance such the dimensional changes, fission gas release in the fuel pins, the burnup profile, fuel centre temperature etc. Evaluation of irradiated structural components and allied materials will provide the essential data for efficient life management of nuclear facilities.

### **Acknowledgement**

The valuable contributions made by Shri S. Anantharaman, Shri N.K. Mondal, Shri D.N. Sah and Shri K.C. Sahoo during different stages of the design, construction and commissioning of this facility is gratefully acknowledged. We also thank Shri Arun Kumar for the support and guidance given during the crucial stages of commissioning of this facility. We are thankful to all the staff members of PIED for carrying out various activities during the project and commissioning stage.

# Microbial Bioremediation of Uranium: an Overview

Celin Acharya  
Molecular Biology Division

## Abstract

Uranium contamination is a worldwide problem. Preventing uranium contamination in the environment is quite challenging and requires a thorough understanding of the microbiological, ecological and biogeochemical features of the contaminated sites. Bioremediation of uranium is largely dependent on reducing its bioavailability in the environment. *In situ* bioremediation of uranium by microbial processes has been shown to be effective for immobilizing uranium in contaminated sites. Such microbial processes are important components of biogeochemical cycles and regulate the mobility and fate of uranium in the environment. It is therefore vital to advance our understanding of the uranium–microbe interactions to develop suitable bioremediation strategies for uranium contaminated sites. This article focuses on the fundamental mechanisms adopted by various microbes to mitigate uranium toxicity which could be utilised for developing various approaches for uranium bioremediation.

## Introduction

Metal contamination cannot be destroyed but can only be concentrated and contained in solid form for final disposal. Bioremediation is an option that offers the possibility to destroy or render the various contaminants harmless using natural biological activity. Microorganisms harbor the potential to restore the metal contaminated environments inexpensively and effectively by employing a number of mechanisms including complexation, binding, reduction, precipitation and accumulation.

Uranium is the heaviest, naturally occurring element found in the earth's crust. It is an alpha emitter and a weakly radioactive element which shows both radiotoxicity and chemotoxicity. However, the chemical toxicity of dissolved uranium is of greatest environmental significance and poses a major concern for public health and safety. Ingestion of high concentrations of soluble uranium compounds manifest in chemotoxic effects on renal tissue leading to kidney failure [1]. Uranium is released in to the environment through its mining, disposal of tailings, nuclear power or weapon production and

nuclear accidents. The mobility of uranium in the environment is dependent on its speciation and its redox state as well. It occurs as U(VI) under oxidizing conditions in the form of a)  $\text{UO}_2^{2+}$  below pH 2.5, b) or hydroxyl complexes below pH 6.5 or c) as uranyl carbonate at  $\text{pH} > 7$  [2]. In the reducing conditions, it exists as insoluble and immobile U(VI) as mineral uraninite. Uranium speciation in contaminated waters is critical for the selection of the treatment process and its successful application. The interactions between microbes and uranium play a very important role in controlling the latter's mobility in natural environment. These interactions can be stimulated to immobilize aqueous uranium thereby remediating the uranium contamination. In microbial systems, no specific mechanism has been attributed to uranium toxicity.

We came across some interesting mechanisms displayed by the microbes to resist uranium toxicity while investigating the microbial interactions with uranium in our laboratory. These mechanisms, harboured by microbes for detoxification of uranium, form the basis of utilization of these organisms for various bioremediation approaches and are discussed below.

### **Adsorption of uranium complexes onto the surface of a unicellular, marine cyanobacterium, *Synechococcus elongatus***

Microbial cells are able to interact with uranium in multiple ways due to diversity in their metabolism and cell surface structures. The latter provide a highly efficient matrix for metal complexation. The metal binding with surfaces of microbial cells is even more efficient than that with inorganic soil components like minerals. The high metal complexation ability of microbial cells is primarily based on two facts: the high surface-to-volume ratio and the usually large number of metal binding ligands, which are presented by the organic cell surface polymers, e.g. peptidoglycan, lipopolysaccharides, proteins and glycolipids. These ligands include functional groups, such as phosphate, carboxyl, hydroxyl, amino and sulfhydryl groups. The adsorption of aqueous metal cations onto these functional groups, the so called biosorption process is rapid, reversible and does not depend on the cell metabolism.

Most of bacterial surface uranyl adsorption studies have focused on low pH conditions where  $\text{UO}_2^{2+}$  is the predominant aqueous uranium species. Above pH 5, neutral and negatively charged uranyl carbonate predominates the aqueous uranium speciation in the marine environment. We investigated the uranium-binding abilities in a marine unicellular cyanobacterium, *Synechococcus elongatus* BDU 75042 from micromolar concentrations of uranyl carbonate at pH 7.8. These cells when exposed to  $23.8 \text{ mg L}^{-1}$  U (or  $100 \mu\text{M}$ ) at pH 7.8 bound 68-72 % U in less than 10 min resulting in a loading of  $53.5 \text{ mg U g}^{-1}$  dry weight [3]. Treatment of U-loaded cells with 0.1 N HCl showed 80 % of U desorption. Most of the bound uranium was found to be associated with the extracellular polysaccharides (EPS) of the cells. The amide groups and the deprotonated carboxyl groups harboured within EPS were likely to be involved in uranyl complexation as suggested by Fourier-transform infrared (FT-IR) spectroscopy.

The X-ray diffraction (XRD) analyses revealed the identity of the uranium deposits associated with the cell biomass as uranyl carbonate hydrate. The uranyl-binding efficiency of the heat killed or the non-viable *Synechococcus* cells was similar to that of live cells, corroborating the metabolism independent bioadsorption of U in these cells [3].

### **Uranium concentration in surface associated polyphosphates in a filamentous, marine cyanobacterium, *Anabaena torulosa***

Uranium has no known biological function and is transported into microbial cells only due to increased membrane permeability (e.g. resulting from uranium toxicity) [4]. There is a lack of direct evidence for the presence of uranium transporters in microorganisms [4]. Therefore, intracellular accumulation of uranium is considered as metabolism-independent process. Bacterial cells have demonstrated several mechanisms to immobilize uranium once it is accumulated intracellularly. One of the known phenomena is uranium chelation by polyphosphate bodies. Inorganic polyphosphates (poly P), are linear polymers of inorganic phosphate (Pi) residues linked by phosphoanhydride bonds. There is a strong evidence for the incorporation of heavy metals into the polyphosphate granules/bodies in several microorganisms.

Our recent studies on the interactions of uranium with a filamentous, heterocystous, nitrogen-fixing marine cyanobacterium, *Anabaena torulosa*, revealed that this strain could sequester uranium in acid soluble polyphosphates, which could be extracted from the cells upon acidification with 1 N HCl at  $100^\circ\text{C}$  [5]. Polyphosphate bodies are generally known to be localized intracellularly in cyanobacterial cells. In the present study, observations using light, fluorescence and electron microscopy-based imaging, coupled with Energy Dispersive X-ray (EDX) spectroscopy and spectrophotometric analyses, have revealed (a) the presence of novel surface associated polyphosphate

bodies (SAPBs) in the filamentous cyanobacterium *A. torulosa* and (b) the interaction of such SAPBs with uranium [5]. When challenged with 23.8 mg L<sup>-1</sup> or 100 μM UO<sub>2</sub>(CO<sub>3</sub>)<sub>2</sub><sup>2-</sup> for 24 h at pH 7.8, under phosphate limited conditions, *A. torulosa* cells bound 65% (15.47 mg L<sup>-1</sup>) of the input U (23.8 mg L<sup>-1</sup>) resulting in a loading of 77.35 mg U g<sup>-1</sup> dry wt. [6]. Backscattered electron SEM image of the uranium loaded cells revealing high contrast spots and the co-occurrence of U and P in the EDX spectra exhibiting such discrete spots suggested the concentration of uranium in such polyphosphate bodies [5]. The co-localization of uranium with the polyphosphate bodies and detachment or extraction of such bodies resulting in large craters on the cell surface accompanied by loss of U and Pi upon HCl based desorption without causing cell lysis, further substantiates their surface association and acid solubility. Uranium immobilization by such surface associated polyphosphate bodies (SAPBs), reported in cyanobacteria for the first time, demonstrated a novel uranium sequestration phenomenon [5].

### **Uranium bioprecipitation by chemo-heterotrophic bacteria isolated from uranium rich deposits**

An alternative strategy for bioremediation under oxygenated conditions is the immobilization of uranium due to the precipitation of hardly soluble inorganic uranium compounds. A well-known mechanism for bioprecipitation of uranium is based on the activity of non-specific phosphatases, in particular, acid and alkaline phosphomonoesterases, which are commonly generated by active soil microorganisms. These enzymes were expressed by a large variety of aerobic and anaerobic bacteria and release inorganic orthophosphate from organic phosphate compounds [7]. As a consequence of this, the released orthophosphate interacts with uranium and causes the precipitation of inorganic uranyl phosphate phases, directly at the cell surface or in the surrounding aqueous system. Beazley and co-

workers [7] demonstrated that the hydrolyzation of organophosphate by aerobic heterotrophic bacteria could play an important role in bioremediation of uranium-contaminated sites.

Domiasiat located in the west Khasi hill district of Meghalaya in Northeast India is one of the largest sandstone-type uranium (U) ore deposits in India containing 9.22 million tonnes of ore reserves with an average ore grade of around 0.1 % U<sub>3</sub>O<sub>8</sub> [8]. This geographically distinct U deposit of Domiasiat is unmined and harbours diverse group of bacteria surviving the stressful environmental conditions prevalent in the ore deposit. Various adaptive features exhibited by the indigenous bacteria from such contaminated sites for their survival under conditions of toxic concentrations of radionuclide and heavy metals have been studied. Representative bacteria (130 isolates- 76 Gram-positive and 54 Gram-negative) were isolated from sub surface soils of such uranium rich deposit and analysed by 16S rRNA gene sequencing [9]. They were affiliated to Firmicutes (51%), Gammaproteobacteria (26%), Actinobacteria (11%), Bacteroidetes (10%) and Betaproteobacteria (2%). Overall, 76% of the characterized isolates revealed phosphatase positive phenotype (phosphatase activity was checked on phenolphthalein diphosphate (PDP) and methyl green agar) and 53% had PIB-type ATPase genes (that detoxify the cytoplasm by effluxing heavy metal ions) [9]. The cultivable bacteria have been reported to tolerate substantial concentrations of U (4 mM) and other metals (Cu, Cd, Pb) and showed potent capacity for binding of U [9,10]. Representative strains removed more than 90% and 53% of U from 100 μM and 2 mM uranyl nitrate solutions, respectively, at pH 3.5 within 10 min of exposure [9]. Two of the representative strains (from the phylum Proteobacteria), *Serratia marcescens* belonging to Gamma proteobacteria and *Burkholderia arbores* belonging to Betaproteobacteria, displayed phosphatase activity. *In vitro* zymogram assay was attempted for both the strains using cell free extracts under acidic and alkaline conditions separately. Under

acidic conditions, active bands at ~80kDa were observed for both the strains whereas under alkaline conditions, active bands at ~58kDa and ~29kDa were seen for *Serratia marcescens* and *Burkholderia arbores* respectively (unpublished results). Assays performed with *Serratia marcescens* ( $OD_{600} \sim 2$ ) with 2mM uranyl nitrate at pH 3.5 in 2mM acetate buffer and 2mM uranyl carbonate at pH 8 in 2mM bicarbonate buffer showed 94% and 80% precipitation of uranium respectively within 72h. Whereas *Burkholderia arbores* under similar conditions precipitated 95% and 89% of U under acidic and alkaline conditions respectively in 72h (unpublished results). Enzymatic precipitation of uranium demonstrated by these naturally occurring, sub surface bacterial isolates from uranium rich deposits reveal the detoxification phenomenon adopted by these isolates to limit uranium toxicity in U and metal contaminated soils.

### Conclusion

Our studies have identified different mechanisms employed by a variety of microorganisms for alleviating uranium toxicity. A fundamental understanding of these mechanisms will prove useful for utilization of these organisms for developing various approaches to uranium bioremediation.

### References

- Gavrilescu M, Vasile L, Cretescu I. "Characterization and remediation of soils contaminated with uranium". *J Hazard Mater* 163 (2009):475-510.
- Choppin G, Liljenzin JO, Rydberg J. Behavior of radionuclides in the environment Radiochemistry Nuclear Chemistry (Third edition), Butterworth-Heinemann, London (2002), pp. 653–685.
- Acharya C., Joseph D., Apte S.K. "Uranium sequestration by a marine cyanobacterium, *Synechococcus elongatus* strain BDU/75042". *Bioresour Technol* 100 (2009):2176-2181.
- Suzuki Y, Banfield JF. "Geomicrobiology of uranium". *Rev Mineral Geochem* 38 (1999): 393–432.
- Acharya C., Apte S.K. "Novel surface associated polyphosphate bodies sequester uranium in the filamentous, marine cyanobacterium, *Anabaena torulosa*". *Metallomics* 5 (2013):1595-1598.
- Acharya C., Chandwadkar P., Apte S.K. "Interaction of uranium with a filamentous, heterocystous, nitrogen-fixing cyanobacterium, *Anabaena torulosa*". *Bioresour Technol* 116 (2012):290-294.
- Beazley M.J., Martinez R.J., Sobecky P.A., Webb SM, Taillefert M. "Uranium biomineralization as a result of bacterial phosphatase activity: insights from bacterial isolates from a contaminated subsurface". *Environ Sci Technol* 41 (2007):5701–5707.
- Sen D.B., Sachan A.S., Padhi A.K., Mathur S.K. "Uranium exploration in the Cretaceous Mahadek sediments of the Meghalaya Plateau". *Expl Res Atom Minerals* 14 (2002):29–58.
- Kumar R., Nongkhaw M., Acharya C., Joshi S.R. "Uranium (U)-tolerant bacterial diversity from U ore deposit of Domiasiat in North-East India and its prospective utilisation in bioremediation". *Microbes and Environ* 28 (2013):33-41.
- Kumar R., Nongkhaw M., Acharya C., Joshi S.R. "Bacterial Community Structure from the Perspective of the Uranium Ore Deposits of Domiasiat in India". *Proc Natl Acad Sci India Sect B Biol Sci* 83 (2013):485–497.



weakened to deep depression by early morning of 13<sup>th</sup> October 2014. According to recent report of IMD<sup>3</sup> the eye of the 'Hudhud' dynamically varied between 30 and 52 km by radius with the progress of time and was around 40 km at the time of landfall. The eye was clearly visible by IR imagery of satellite at 05:30 IST on 11<sup>th</sup> and continued to be present till 14:30 IST of 12<sup>th</sup> October 2014. The centre of eye was at about 50 km North-North-East of BARC, Visakhapatnam. Maximum storm surge of 1.4 m above the astronomical tide was observed at the tide gauge installed at Visakhapatnam (IMD<sup>3</sup>).



**Fig.2: BARC, Visakhapatnam site embedded with hills and hillocks and nearby meteorological stations**

**Wind field**

The maximum 1 minute sustained surface wind speed was 137 km/h at AWS Visakhapatnam (IMD<sup>3</sup>). According to interpretation of satellite imageries, as per Dvorak technique by the IMD, VSCS 'Hudhud' was T5.0 on intensity scale, which corresponds to a maximum sustained wind speed of about 167-185 km/h. Maximum gale wind has been captured by an AWS installed at a ship near Visakhapatnam port. This has recorded one-minute average Maximum Sustained Wind (MSW) of 182 km/h at the time of landfall

on 12<sup>th</sup> October 2014 (IMD<sup>3</sup>).

Hourly 3 minute snapshot of meteorological parameters measured by Automatic Weather Station (AWS) at Anakapalle (IMD<sup>4</sup>) and in house ERM-AWS station installed at BARC, Visakhapatnam (Vinod Kumar<sup>2</sup>) both measuring 7 m in height (near surface) are the observatories to analyze 'Hudhud' at BARC, Visakhapatnam. Crow fly distance between these two observatories is around 20 km in and around the cyclone track (Fig. 2). In addition, as shown in Fig. 2, there is an in-house unit of Ultrasonic Anemometer (UA) station installed at the foothill of Gandivanipalem near security gate of BARC, Visakhapatnam (situated around 3 km NNE of ERM-AWS, BARC, Visakhapatnam). This has captured half-hourly averaged wind speed, wind direction, atmospheric temperature and relative humidity at measurement height of 4 m from surface. First peak of maximum surface wind speed, 79 km/h has been noted by ERM-AWS at BARC, Visakhapatnam at 12:30 h (IST) around the landfall of 'Hudhud'. At that time 80 km/h wind speed has been recorded by AWS, Anakapalle as 3 minute averaged data (IMD<sup>4</sup>). Maximum wind speed, 87 km/h has been recorded at Anakapalle around 13:30 h (Fig. 3). At this time

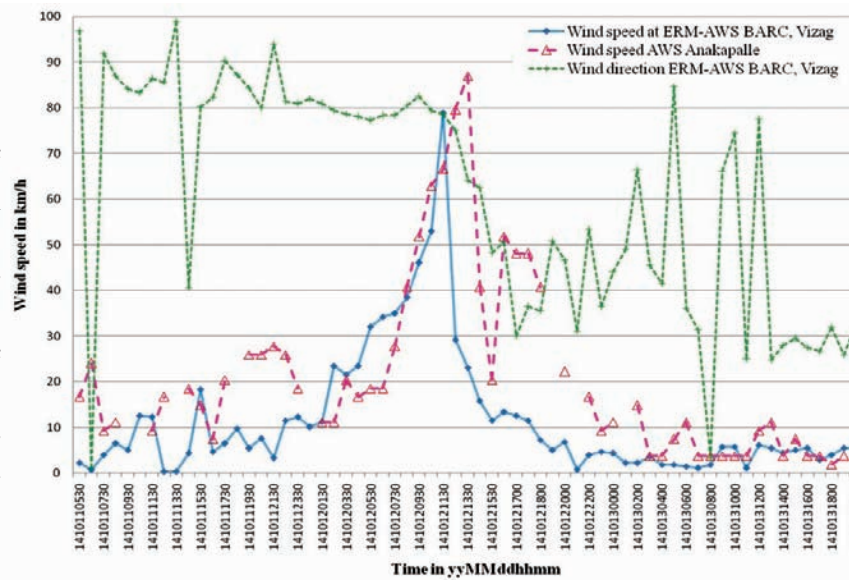


**Fig.3: Hourly 3 minute instantaneous wind speed and wind direction captured by AWS, Anakapalle and ERM-AWS at BARC, Visakhapatnam.**

ERM-AWS at BARC, Visakhapatnam recorded a value of 29 km/h.

Gradual increase in 3 minute gusty wind speed been recorded at AWS stations since 03:30 h on 12<sup>th</sup> October 2014 (Fig. 3) as soon as SCS form of Hudhud has been intensified and drifted Westerly to hit Visakhapatnam coast to be VSCV at 07:30 h. At that time, surface wind speed recorded at AWS, Anakapalle was 27 km/h and at AWS, BARC, Visakhapatnam it was around 12 km/h. BARC, Visakhapatnam is always under hill shadow zone mostly for North-Easterly and Northerly wind as the terrain is a coastal pocket of the mountainous zone of Eastern Ghats. This phenomenal behaviour, through wind speed has been reflected at UA station installed at foothill of a 155 m tall hill at Gandivanipalem BARC, Visakhapatnam (Fig. 4). Two incidents of gusty cyclonic wind have been experienced before and after landfall of 'Hudhud' in and around cyclonic eye at coast during the period 07:30 – 17:30 hour as recorded by AWS Anakapalle (Fig. 3). At BARC, Visakhapatnam gusty wind has mostly appeared in post landfall period as indicated by the variation in wind direction of ERM-AWS, at BARC, Visakhapatnam. Wind field of 'Hudhud' has been significantly broken after entering into land

after landfall and shortly converted to SCS (Fig. 1). Phenomenal behavior of cyclonic storm has been well captured by anticlockwise rotation of wind as shown in IR image of INSAT 3D (Fig. 5) at 14:30 h after 3 hours of landfall. However, SCS form of 'Hudhud' after landfall has caused sharp rise in 30 minute averaged wind speed at UA station at Gandivanipalem. A very strong gusty horizontal wind shear recorded by UA during 13:00-16:30 h (Fig. 4) after turning of the wind from North-westerly to Westerly and further

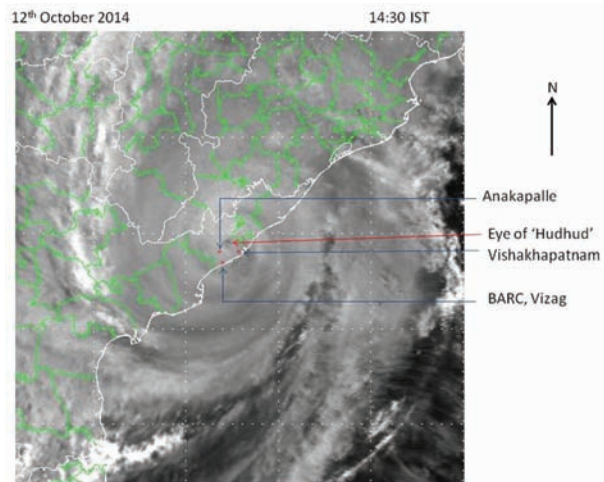
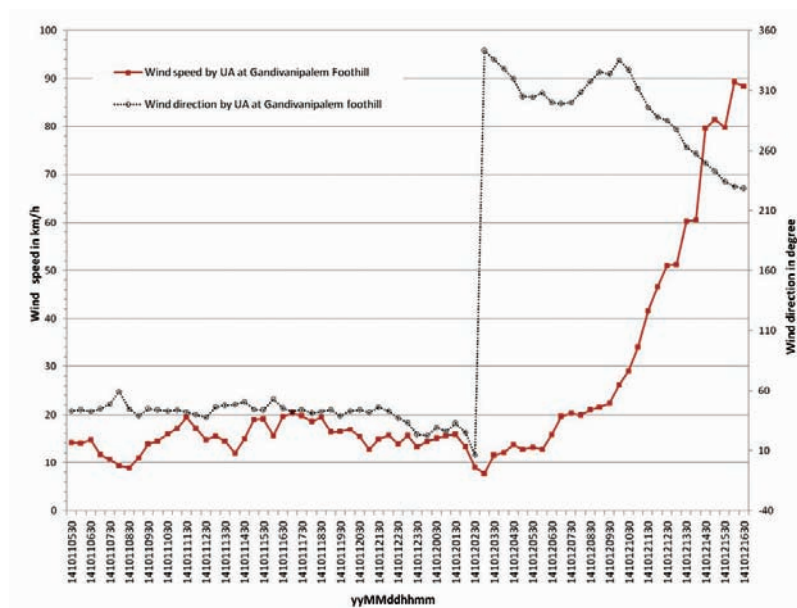
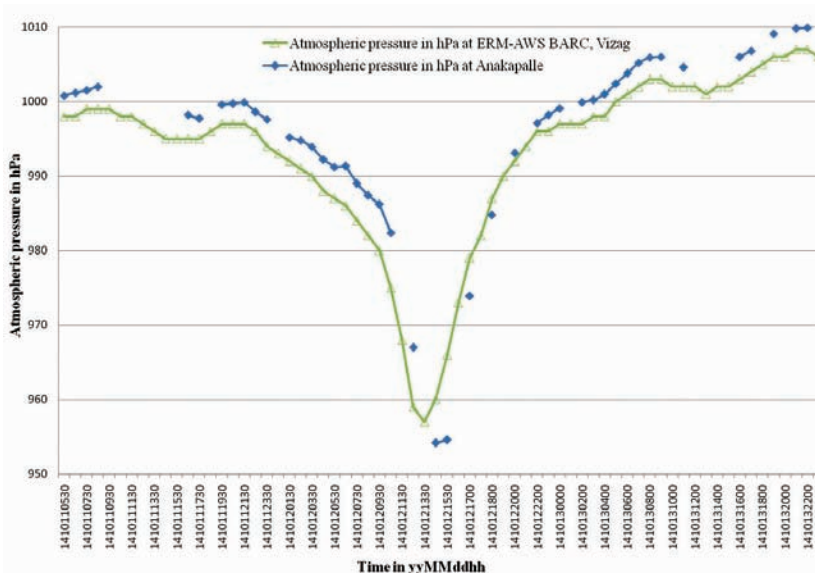


Fig.5: Satellite IR image of Very Severe 'Hudhud' at 14:30 IST on 12<sup>th</sup> Oct. 2014 after landfall.



**Atmospheric Pressure**

Lowest atmospheric pressure has been recorded at 12:30 h by ERM-AWS, at BARC, Visakhapatnam just after land fall of ‘Hudhud’ with recorded lowest atmospheric pressure, 957 hPa (Fig. 6). Pressure fall was around 44 hPa below normal. Lowest atmospheric pressure has been recorded at 14:30 h by AWS, Anakapalle after 3 hours of land fall of ‘Hudhud’ with recorded lowest atmospheric pressure, 954 hPa (IMD<sup>4</sup>). West-North-Westerly movement of ‘Hudhud’ was closest to Anakapalle around 14:30 h of the day (Fig. 5 and 6). As registered by IMD<sup>3</sup>, minimum atmospheric pressure of ‘Hudhud’ was 950.3 hPa at the coast of Visakhapatnam at the time of landfall.



**Fig.6: Hourly atmospheric pressure observed by AWS, Anakapalle and ERM-AWS, BARC, Visakhapatnam.**

**Net Radiation due to Solar Insolation**

Daytime net radiation range on 12<sup>th</sup> October was between (-)170 W/m<sup>2</sup> and (+)3 W/m<sup>2</sup> indicating overcast condition throughout the day. With this observation, it is concluded that BARC, Visakhapatnam did not witness bright sunshine which is a phenomena of geo-location of eye of the cyclone, i.e., eye of Hudhud did not reach BARC, Visakhapatnam. This was witnessed in Visakhapatnam causing maximum

damage by wind shear at eye-wall of Hudhud due to near Westerly movement of the eye of VSCS form of Hudhud.

**Ambient Temperature**

Range of ambient temperature during this period was 23.1-30.2 °C. The highest temperature was recorded at 12:00 h on 11<sup>th</sup> October. The lowest temperature was recorded at 13:30 h by ERM-AWS, at BARC, Visakhapatnam just after land fall of Hudhud on 12<sup>th</sup> October. Temperature (30 minute average) was below 24°C at UA station, Gandivanipalem during 14:00-16:00 h on same day (Fig. 7). Lowest temperature, 23.4°C was recorded by AWS, Anakapalle at 11:30 h around the landfall (IMD<sup>4</sup>). The site was under cold core zone of southern part of ‘Hudhud’.

**Relative Humidity and Rainfall**

Measured relative humidity was above 90% during 08:30 - 21:00 h on 12<sup>th</sup> Oct.2014. 32.4 cm rainfall was recorded at BARC, Visakhapatnam site during the period 11<sup>th</sup> October 2014: 21:30 h to 12<sup>th</sup> October 2014 : 20:30 h. It is about 23% of annual total rainfall of Visakhapatnam district. 7.6 cm rainfall has been received at BARC, Visakhapatnam before the landfall of ‘Hudhud’. 22.5 cm rainfall has been received during 12:30 -16:30

h on 12<sup>th</sup> October 2014 as recorded by raingauge at BARC, Visakhapatnam (Fig. 7). During this period relative humidity (recorded at Gandivanipalem) was above 95%. Reported rainfall at Anakapalle raingauge was 18 cm during 12<sup>th</sup>, 8:30 IST to 13<sup>th</sup>, 8:30 IST October 2014. In the recent report of IMD<sup>3</sup> it is stated that rain-bearing cloud band encircled the complete southern part by 10:00 IST of 12<sup>th</sup> October 2014. Satellite imagery has shown the same (Fig. 5).

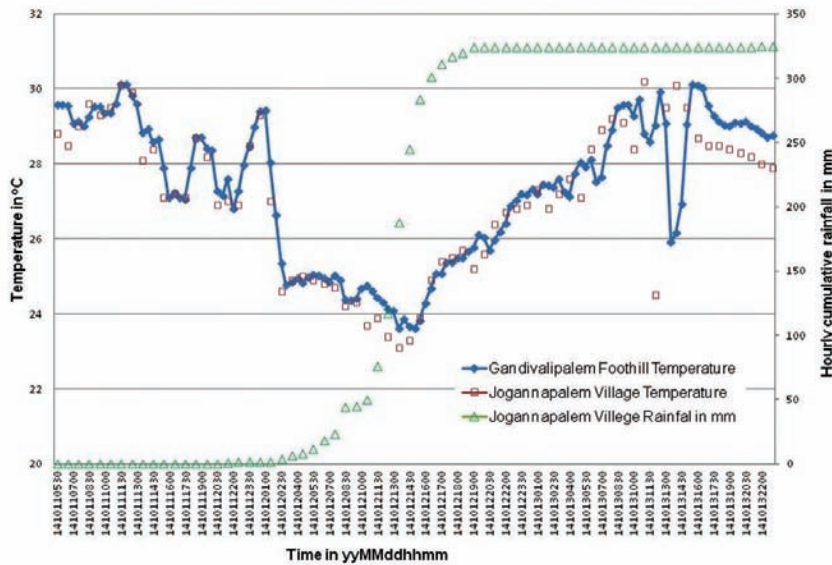


**Fig.7: Hourly ambient temperature and cumulative rainfall observed at BARC, Visakhapatnam.**

The outer band caused heavy rainfall activity along the coast of north Andhra Pradesh and adjoining coastal Odisha from the afternoon of 11<sup>th</sup> October 2014.

**Conclusion**

Landfall of a tropical cyclone at Visakhapatnam was one of the rarest events experienced after 29 years. Eye of the VSCS was 40 km wide at the time of landfall between 11:30 and 12:30 IST on 12<sup>th</sup> October 2014. Maximum 30 minute averaged sustained wind speed was 89 km/h at BARC, Visakhapatnam site as recorded by fast response 3D sensors of Ultrasonic Anemometer. BARC, Visakhapatnam site has faced relatively lower impact of this natural disaster being at southern part of phenomenal tropical cyclone

with wind breaking factors of hills and hillocks at the site. Maximum atmospheric pressure fall was around 54 hPa. Atmospheric pressure fall was 44 hPa than the normal at BARC Visakhapatnam site. The recorded minimum pressure at BARC site was 957 hPa at the time of landfall. Rainfall at site due to the event was 32.4 cm.

**Acknowledgement**

Support extended by Regional Director, BARC Facilities, Visakhapatnam is gratefully acknowledged.

**References**

1. Jana R, Vinod Kumar A, Krishna N S and Sambamurty T. "Summary report of surface meteorology at Jogannapalem area of BARC-Visakhapatnam for the observation period October 2011-December 2013". BARC Technical Report, BARC/2014/I/006, (2013): 1-130.
2. A Vinod Kumar, M P Ratheesh, S S Salunkhe, R Jana, S G Gavas, T Mukundan, P R Ninawe, M S Prakasha, S Garg and M D Patel. "Design and development of an integrated environmental Radiation Monitor - Automatic Weather Station (ERM-AWS)". *BARC Newsletter*, May-June, (2014): 34-37.
3. IMD "Very Severe Cyclonic Storm, HUDHUD over the Bay of Bengal (07-14 October 2014): A Report". Cyclone Warning Division, IMD, (2014): 1-66.
4. IMD. <http://www.imdaws.com/ViewAwsData.aspx>, (Accessed during 11<sup>th</sup> - 14<sup>th</sup> October 2014).

## Third National Symposium on Advances in Control and Instrumentation (SACI- 2014): a Report

SACI-2014 was organized by the Reactor Control Division, BARC and was sponsored by the Board of Research in Nuclear Sciences (BRNS). It was held at the NPCIL auditorium, Nabhikiya Urja Bhavan, Anushaktinagar, Mumbai from November 24-26, 2014. The Symposium comprised ten sessions and 10 invited talks from subject experts. A total of 97 papers presented at the oral and poster sessions of the symposium, spanning a wide range of topics such as control theory, Control and Instrumentation (C&I) architecture applications and experiences, advances in tools and techniques, sensors, software security etc.

SACI 2014 was marked by active participation of a large number of delegates from various R&D institutions, industry and academia. SACI-2014 played a synergizing role in shaping the architecture of next generation C&I Systems in India. It also presented an opportunity to showcase Indian achievements and advances in the Control & Instrumentation sector and served as a platform to converge upon strategies in addressing future challenges in C&I sector such as rapid obsolescence of tools, techniques and components and ever-increasing demands in C&I software security.



Release of Book of Abstracts & Proceedings of SACI-2014: (L-R): Shri Y.S. Mayya, Head, RCnD & CnID and AD, E&I Grp., BARC, Shri C.K. Pithawa, Director, E&I & DMA Grps., BARC, Shri K.C. Purohit, C&MD, NPCIL, Dr. Sekhar Basu, Director, BARC, Shri A.G. Apte, Chairman, National Technology Research Organization, Dr. M.Y.S. Parsad, Director, Satish Dhawan Space Centre, ISRO and Dr. A.P. Tiwari, Outstanding Scientist, RCnD, BARC

## 29<sup>th</sup> Training Course on “Basic Radiological Safety and Regulatory Measures for Nuclear Facilities”: a Report

The BARC Safety Council (BSC) Secretariat conducts series of short term training courses on “Basic Radiological Safety and Regulatory Measures for Nuclear Facilities” for the staff members of BARC to impart general awareness on basic radiological, industrial safety aspects and regulatory requirements. In this series, the BSC Secretariat conducted the 29<sup>th</sup> Training Course at BARC, Tarapur during March 02-05, 2015. The inauguration of this training programme was held on 2<sup>nd</sup> March 2015, at SFSF Auditorium, BARC, Tarapur. Shri Jose Joseph, Head, BARC Safety Council Secretariat welcomed the dignitaries and participants and introduced the contents of various courses of the training programme and their relevance. He explained the importance of regulatory measures in controlling the radiation exposure and adherence to safety procedures. The Chief Guest of the function Shri G.P. Srivastav, Former Chairman, BSC and Former Director, E&I Group in his remark emphasized the safety aspects and strict adherence to regulatory codes, guides and recommendations. He advised the participants to avail the benefits of this programme and to share the knowledge with others working with them. He appreciated the efforts of BSCS for conducting these courses for officers of BARC, Tarapur. The inaugural

function was graced by Shri S. Pradhan, CS, TNRPO and Shri DAS Rao, PD, INRP, Tarapur and other senior officials of NRB, BARC, Tarapur. The vote of thanks was proposed by the Course Director, Shri R.P.Hans, BSCS.

The training course was organized by Shri R.P.Hans, Shri C.L.R.Yadav, Smt. E. Sumathi and Shri S. Deolekar and other officers of BSCS. About 50 participants from NRB, BARC, Tarapur and AFFF, Tarapur attended the course. The training programme was conducted through classroom lectures and demonstrations. Faculty members were specialists with many years of experience from BSCS, HPD, RSSD, MD, IHSS, NPCIL and Fire Services Section. The training programme covered various aspects of safety including topics such as contamination and contamination control in fuel reprocessing and fabrication facilities, environmental radiation monitoring around nuclear facilities, occupational health care and management of internal contamination, preparedness and response to nuclear and radiological emergencies and safety framework for BARC etc. Two specific lectures were also delivered on Off-site Emergency Response and Preparedness around NPPs, Tarapur and Lesson learned from Criticality Accident at Tokaimura, Japan.



Dignitaries on the dais are Chief Guest, Shri G.P. Srivastav, Former Chairman, BSC, Shri Jose Joseph, Head, BSCS, Shri S. Pradhan, CS, TNRPO, Shri DAS Rao, PD, INRP and Shri R.P.Hans, Head, SR & RSS, BSCS

## National Safety Day Celebration at BARC

As part of continuing health and safety promotional activity of the Industrial Hygiene and Safety Section, Health Safety and Environment Group (HS&EG), National Safety Day was celebrated at the Centre on March 5, 2015 at the Central Complex (CC) Auditorium.

The day-long programme commenced with the participants taking the Safety Pledge read by the guests of honour Shri R.J. Patel, Chairman, CFSRC and Shri R.P. Raju, Controller, BARC. Shri S. Soundararajan, Head IHSS, spoke about the methodology of selection of the award-winning safety slogans and posters and thanked the committee which was constituted for this task.

Shri R.P. Raju reiterated that accidents were preventable through appropriate control measures and by adopting safe practices. Shri R.J. Patel, in his address, stressed the importance of dissemination of health and safety related information. He appreciated the staff of the Industrial Hygiene and Safety Section for putting up concerted efforts in improving the safety status of this institution. The winners of safety posters and safety slogan competitions were awarded prizes by the guests of honour. Later, Shri R.J. Patel inaugurated the Safety Poster Exhibition arranged at the CC Auditorium. As part of the programme safety films were also screened.



Shri R.J. Patel, Chairman, CFSRC inaugurating the Safety Poster Exhibition  
Inset: Shri R.P Raju, Controller, BARC and Shri R.J. Patel, addressing the gathering

## BARC Scientists Honoured

Name of the Scientists : Pramod Bhatt and S. M. Yusuf  
Affiliation : Solid State Physics Division, BARC  
Name of the Award : Best Poster Award  
Title of the Paper : Neutron Diffraction Study of the Chain Molecular Magnet  $[\{Co_{II}(\Delta)Co_{II}(\Lambda)\}(ox)_2(phen)_2]_n$   
Presented at : 5<sup>th</sup> Conference on Neutron Scattering (CNS-2015), held at Homi Bhabha Centre for Science Education, Mumbai, during 2-4 February, 2015.

Name of the Scientist : Jhimli Paul Guin  
Affiliation : Radiation Technology Development Division, BARC  
Name of the Award : Best Poster Award (2<sup>nd</sup> Prize)  
Title of the Paper : Radiation Crosslinked Graphene/Polymer Nanocomposites for Controlled Orotransmucosal Delivery of Doxycycline  
Presented at : DAE-BRNS 5<sup>th</sup> Interdisciplinary Symposium on Materials Chemistry (ISMC-2014), Mumbai, December 9 -13, 2014.



Modular Lab at BARC

Edited & Published by:  
Scientific Information Resource Division  
Bhabha Atomic Research Centre, Trombay, Mumbai 400 085, India  
BARC Newsletter is also available at URL:<http://www.barc.gov.in>